11

Echocardiography in the Adult with Congenital Heart Disease

Julie A. Kovach

Key Points

- Echocardiography, because of its excellent spatial resolution and ability to assess both anatomy on two-dimensional imaging and physiology by Doppler, is especially suited to the diagnosis and follow-up of adults with congenital heart disease.
- Indications for echocardiography in this patient population have been published.
- In the previously undiagnosed adult with suspected congenital heart disease, a careful segmental approach to scanning is required to make a complete diagnosis.
- Echocardiography of adults with congenital heart defects should be performed and interpreted by personnel trained in the care of these patients.
- Echocardiography of adults with congenital heart disease requires knowledge of the anatomy and natural history of unoperated defects, awareness of the possible palliative or corrective procedures for the defect, and awareness of the potential complications, sequelae, and residua of the repair.

Indications for Echocardiography in the Evaluation of the Adult with Congenital Heart Disease

Thanks to advances in antenatal and postnatal diagnostic methods, rapid progress in surgical options and technique, improvements in perioperative management, and meticulous care by pediatric cardiac specialists, over 85% of children born with cardiac anomalies survive well into adulthood. The 32nd Bethesda Conference sponsored by the American College of Cardiology estimated that over 800,000 adults with congenital heart defects were living in the United States as of the year 2000.[1] Based on birth rates and disease incidence, one group of investigators estimated that there are currently up to 1.33 million U.S. survivors with congenital heart disease born since 1940, 56% with simple lesions, 30% with moderately complex lesions, and 14% with more severe lesions.[2] An additional 3 million Americans have bicuspid aortic valves. Adults, most of whom have undergone some operation to repair or palliate their defect, will soon outnumber children with congenital cardiac defects. The long-term clinical course of these patients will be determined by both their congenital and acquired cardiovascular conditions, which require accurate diagnosis, diligent ongoing follow-up, and continued management.

Echocardiography plays an essential role in the diagnosis and management of patients with congenital heart disease. For an unselected cohort of children and adolescents referred for evaluation of a cardiac murmur, echocardiography identified congenital cardiac lesions in 12% of subjects diagnosed to have a functional murmur on history and physical examination performed by experienced congenital cardiologists. For 152 individuals who underwent auscultation, the diagnosis by echocardiography was discordant in 19% of patients, with a major discordance recorded in 6%.[3] In many cases, echocardiography supplants invasive diagnostic techniques in patients who proceed to complete repair, palliation, or reoperation without the need for cardiac catheterization. Transthoracic echocardiography (TTE) with two-dimensional (2D) imaging and color[4] and spectral Doppler affords accurate and complete characterization of cardiac anatomy and hemodynamics in the majority of adults with congenital heart disease. For patients with limited acoustic windows due to

prior operations, body habitus, coexistent lung disease, or atypical cardiac location within the chest, or those with structures not accessible to TTE, transesophageal echocardiography (TEE) provides direct visualization with excellent resolution.[5–8] In the operating room, TEE provides invaluable assistance to the surgeon in determining the nature of the surgery, assesses adequacy of repair, and rapidly identifies any immediate complications, thus reducing operative morbidity and mortality.[9,10] Interventional cardiologists use TEE or intracardiac catheter-based echocardiography for guidance during transcatheter procedures, especially for placement of closure devices for atrial septal defects (ASD) or patent foramen ovale (PFO).[11–17] Three-dimensional echocardiography, a promising technique with rapidly improving image quality and speed of image acquisition and rendering, has added to the understanding of congenital heart disease, including ASD closure, and facilitated the diagnosis of cor triatriatum, an uncommon congenital defect.[18–22] Diagnosis of cardiac abnormalities in utero by fetal echocardiography promotes better counseling and education of families. In addition, fetal echocardiography facilitates earlier planning of postnatal management by physicians and parents, including possible surgery.[23]

Adults with previously undiagnosed congenital cardiac defects, many with minimal hemodynamic consequences up to that time, require a similar echocardiographic approach to that called for in children. It is not unusual for a small ASD without significant left-to-right shunt to be first diagnosed on routine TTE performed for other indications. However, important differences exist between most adults with previously diagnosed or repaired congenital heart defects and their pediatric counterparts, and these differences necessitate additional considerations for the acquisition and interpretation of echocardiographic images in these patients. Adults typically have more difficult acoustic windows with less clear images than children owing to larger body size, prior surgeries, and coexisting conditions that can affect image quality such as lung disease. Echocardiographic contrast agents may improve diagnostic accuracy for assessment of ventricular function and diagnosis of certain anomalies such as apical hypertrophic cardiomyopathy or noncompaction of the left ventricle in these patients.[24] Age- and body habitus–associated changes in cardiac position within the chest, cardiac malposition at baseline, or the presence of conduits may require the use of multiple imaging planes from varied ultrasound transducer positions on the chest wall that differ from standard transducer locations. "Adult" cardiovascular diseases like hypertension and atherosclerotic coronary or peripheral arterial disease may alter the "typical" physiology of a congenital defect; for example, a small secundum ASD with no significant shunt when the patient is 20 years of age may cause right ventricular volume overload at age 50 when blood pressure is higher and ventricular compliance is less. Patients with unoperated cardiac lesions will exhibit expected complications of that defect as determined by the underlying lesion. Importantly, adults with congenital abnormalities that were "successfully" repaired or palliated in childhood, including adults with "cured" ASD and coarctation of the aorta, may have residua or late complications of the repair or sequelae of unrepaired components of the defect. The echocardiographer must have knowledge of the echocardiographic features of the isolated unrepaired defect, understand the potential repairs or corrective operations for each defect (especially since the patient may not know the nature of his operation), and examine for potential complications, residua, or late sequelae of unoperated defects or surgical repair or palliation. Thus, echocardiography in the adult with congenital heart disease demands a thorough and careful systematic approach.

This chapter emphasizes the general approach to the examination, outlines echocardiographic features of common defects that may first appear in adulthood, briefly reviews the echocardiographic characteristics of lesions that were most likely diagnosed and operated in childhood, presents the usual appearance of standard operative (and transcatheter) procedures for congenital cardiac anomalies, and demonstrates the echocardiographic findings of the most common late complications or sequelae of palliation or correction. Both 2D TTE and TEE have widespread use in these patients and are presented in detail. M-mode echocardiography, which at one time was utilized for the diagnosis of certain cardiac defects, has minimal clinical application at present and is not discussed. Like pediatric patients, adults with previously undiagnosed congenital heart anomalies benefit from a sequential, segmental approach for the determination cardiac anatomy.

Indications and General Segmental Echocardiographic Approach

The American College of Cardiology/American Heart Association Task Force on Practice Guidelines (Committee on Clinical Applications of Echocardiography) noted the following reasons for adult congenital patients to seek care from a cardiologist and for which they might need an echocardiogram: (1) an initial diagnosis of congenital heart disease; (2) a previously recognized congenital heart disease that is presently inoperable; (3) a progressive clinical deterioration, such as ventricular dysfunction or arrhythmias due to the natural history of their defect; (4) the patient becomes pregnant or has other stresses such as noncardiac surgery or infection, including infective endocarditis; (5) the patient has residual defects after a palliative or corrective operation; (6) the patient develops arrhythmias (including ventricular tachycardia, atrial flutter, or atrial fibrillation) that may result in syncope or sudden death; (7) a progressive deterioration of ventricular function with congestive heart failure; (8) progressive hypoxemia because of the inadequacy of a palliative shunt or the development of pulmonary vascular disease; or (9) the patient requires monitoring and prospective management to maintain ventricular or valvular function or to prevent arrhythmic or thrombotic complications. The task force recommended that cardiac sonographers and physicians who perform and interpret echocardiograms for these patients have special competency in congenital heart disease or refer the patient to a cardiologist (either adult or pediatric) who is trained in the care of adults with congenital heart disease. Based on these considerations and the available literature, the task force issued guidelines for indications for the performance of 2D and Doppler echocardiograms in the adult patient with congenital heart disease (Table 11.1).[25]

TABLE 11.1. Indications for echocardiography in the adult patient with congenital heart disease

Class I	Patients with clinically suspected congenital heart disease, as evidenced by signs and symptoms
	Patients with known congenital heart disease when there is a change in clinical findings
	Patients with known congenital heart disease for whom there is uncertainty as to the original diagnosis or when the precise nature of the defect is unclear
	Periodic echocardiograms in patients with known congenital heart disease for whom ventricular function and atrioventricular valve regurgitation must be followed
	Patients with known congenital heart disease for whom pulmonary artery pressure is important
	Periodic echocardiography in patients with surgically repaired or palliated congenital heart disease with the following: change in clinical condition, clinical suspicion of residual defects, left or right ventricular function that must be followed, the possibility of hemodynamic progression, or a history of pulmonary hypertension
	To direct interventional catheter valvotomy (or other interventions as necessary) in the presence of complex cardiac anatomy
Class IIb	Annual or biennial follow-up Doppler echocardiographic study in patients with known hemodynamically significant congenital heart disease and no evident change in clinical condition
Class III	Multiple repeat Doppler examinations in a patient with repaired patent ductus arteriosus, atrial septal defect (ASD), ventricular septal defect (VSD), coarctation of the aorta, or bicuspid aortic valve without change in clinical condition
	Repeat Doppler examinations in patients with known hemodynamically significant congenital heart lesions

In general, the echocardiographic approach to the previously undiagnosed patient is anatomically sequential following the course of blood flow through a normal heart and focusing on the presence or absence and location of cardiac structures, with attention to morphology, relationships and connections to one another. This approach is summarized below. The sonographer must recognize that standard imaging planes may not be helpful and adapt scanning as necessary. "Unusual" transducer positions, including high parasternal, laterally displaced apical, and even right-sided or posterior thorax locations may be required to image certain structures. Importantly, the ultrasound plane should be purposefully aligned to visualize a specific structure of interest. For previously operated patients, the cardiac sonographer must have knowledge of possible types of repairs for a particular anatomic defect and use whatever clues are available to examine the repair if the patient does not know the nature of her surgery. For example, an adult with tetralogy of Fallot who has an isolated scar on the right lateral thorax and no right radial pulse may have been palliated in childhood with a Blalock-Taussig shunt, and therefore might need a right supraclavicular transducer position with Doppler to evaluate for shunt obstruction and to estimate pulmonary artery pressure. Finally, the examination must include sufficient views to evaluate all intracardiac and extracardiac structures, the normality or abnormality of these structures, and the hemodynamic consequences of anatomic alterations. The patient should not leave the laboratory until every attempt has been made to answer all the questions.

The first step of the examination, especially in the previously undiagnosed patient, is to determine visceral and atrial situs and cardiac position within the chest (normal or levocardia, dextrocardia, or mesocardia). This is most easily accomplished from a subcostal transducer position and transverse imaging plane in the upper abdomen. Since atrial situs and visceral situs are usually concordant, a right-sided liver and inferior vena cava and left-sided gastric bubble and aorta are almost always associated with atrial *situs solitus*, whereas a left-sided liver and right-sided gastric bubble indicate atrial *situs inversus*. Since visceral-atrial discordance is almost always accompanied by complex congenital defects, it is usual that that diagnosis would already have been made in childhood, so this is of little concern in the previously undiagnosed adult. Additional clues to the determination of atrial situs include the presence of the inferior vena cava draining into an atrium (almost always the right atrium) and atrial morphology. Some patients have an absent inferior vena cava associated with anomalous drainage into the azygous vein in the right chest, so the absence of the inferior vena cava on ultrasound is not helpful in determining atrial situs. The right atrium is broad-based and triangular ("puppy dog's ear" appearance) and is associated with a eustachian valve while the left atrium is narrow-based, longer ("finger" appearance), and is not associated with a eustachian valve. In addition, the septal surface of the left atrium contains the flap valve of the fossa ovalis. Rare patients have bilateral right or left atria (isomerism) or have a common atrium with no atrial septum.

Second, both systemic and pulmonary venous connections to the atria should be determined. In adults, only three pulmonary veins are generally visualized on TTE (best seen in the apical views). The right inferior pulmonary vein is not seen. All pulmonary venous drainage into the left atrium can be easily identified on transesophageal imaging. Third, abnormalities of ventricular inflow such as tricuspid atresia or cor triatriatum are assessed. Fourth, ventricular number, morphology, relative size, position, and concordance with the atria are determined. A ventricle is defined as a chamber that receives at least 50% of the ventricular "inlet" or fibrous ring of the atrioventricular (AV) valve. Neither AV valve patency nor connection to an outlet is required. Chambers that do not meet these criteria are termed rudimentary chambers and may or may not have an outlet. The number of ventricles is determined by the presence or absence of an interventricular septum. If only one ventricle is present (e.g., double inlet left or right ventricle, possibly tricuspid atresia, etc.), the morphology of the ventricle should be classified as right, left, or indeterminate. Of note, the ventricle is almost always concordant with the AV valve. That is, a tricuspid

valve (three leaflet with chordal attachments to three papillary muscles) regulates flow into a right ventricle, and a mitral valve (two leaflets with chordal attachments to two papillary muscles) regulates flow into the left ventricle. The septal leaflet of the tricuspid valve inserts more apically than the anterior leaflet of the mitral valve. The right ventricle is generally heavily trabeculated while the left ventricular endocardial surface is smooth. The presence of a moderator band defines a right ventricle. Fifth, abnormalities of cardiac septation such as ASD, ventricular septal defect (VSD), and AV septal defect (AV canal or endocardial cushion defect), including direction and magnitude of shunt, are assessed.

Sixth, ventriculoarterial concordance and great vessel number and relationships are elucidated. Normally, the morphologic right ventricle is anterior and to the right of the morphologic left ventricle and gives rise to a pulmonary artery that is anterior and to the left of the aorta. The morphologic left ventricle gives rise to an aorta that is posterior and to the right of the pulmonary artery. Since the great arteries normally arise in orthogonal planes, their long axes are perpendicular on echocardiogram. In the parasternal and subcostal short axis views, the aorta and aortic valve appear in short axis posterior and to the right of the pulmonary artery and right ventricular outflow tract, which are visible in long axis, the typical "circle and sausage" appearance. In the two forms of ventriculoarterial discordance (transposition complexes), the great arteries arise in parallel; thus, both appear as "circles" with varied anteroposterior and lateral relationships in the parasternal short axis and in longitudinal plane in the parasternal long axis views, respectively. In *d*-transposition of the great arteries, the atria and ventricles are concordant with normal anteroposterior and right-left position of the ventricles, but the aorta arises anteriorly from the right ventricle. The pulmonary artery arises posteriorly and then bifurcates, an appearance readily identified on echocardiogram and key to differentiating the two great arteries. In *l*-(congenitally corrected) transposition, there is atrioventricular and ventriculoarterial discordance, so that the morphologic right ventricle lies posterior and to the left of the left ventricle and gives rise to an aorta while the morphologic left ventricle lies anterior and to the right and gives rise to a pulmonary artery. This often is best thought of as "ventricular inversion" since there is no mixture of deoxygenated and oxygenated blood in the isolated form of this defect and patients are not cyanotic.

Seventh, the right and left ventricular outflow tracts, including subvalvular, valvular, supravalvular, and distal great arteries must be evaluated for the presence of obstructive lesions such as pulmonary valve stenosis, branch pulmonary artery stenosis, discrete subaortic membranes, and even coarctation of the aorta. Finally, attention is turned to the evaluation of native shunts (e.g., patent ductus arteriosus, aortopulmonary windows, ruptured sinus of Valsalva aneurysm, or systemic to pulmonary artery collaterals), and postoperative structures (patches, conduits, surgically created systemic to pulmonary shunts, Fontan circuits, etc.). In some younger adults with excellent acoustic windows, origins of coronary arteries can be identified in the parasternal short axis view.

Abnormalities of Cardiac Septation

Atrial Septal Defect

The most commonly diagnosed congenital cardiac defect in adulthood, aside from bicuspid aortic valve, is ASD, which accounts for almost 30% of all first congenital cardiac diagnoses in adults. It occurs due to failure or incomplete development of portions of the interatrial septum and is classified by the embryologic segment of the septum involved by the defect. The ostium primum ASD, actually a type of endocardial cushion defect often called a "partial" AV canal, is characterized by the absence of the primum septum at the AV junction or crux of the heart, is usually accompanied by abnormalities of the anterior mitral valve leaflet in the form of a cleft, and represents approximately 15% of ASD in adults. Approximately 75% of ASDs are of the ostium secundum type, which is caused by a defect in portions of the membranous fossa ovalis (secundum septum). The atrial septal aneurysm, which may be congenital or acquired, occurs when the membranous flap of the fossa ovalis protrudes with a "windsock"-like appearance into one or the other atrium and may demonstrate mobility during the cardiac cycle. Atrial septal aneurysms may have multiple small fenestrations that are not visible on color Doppler. Occasionally, especially if a PFO or multiple fenestrations are present with right-to-left shunt, an aneurysmal atrial septum may be associated with paradoxical embolization. Patent foramen ovale, persistence of the normal embryologic state of an open flap valve of the fossa ovalis, occurs in approximately 20% to 25% of all adults, is not due to absence of atrial septal tissue, and should not be confused with ASD. As noted previously, PFO, especially in patients with atrial septal aneurysm, may be associated with paradoxical thromboembolism. Sinus venosus ASD, caused by absence of the basal segment of the interatrial septum most commonly at the superior vena cava (SVC) and rarely at the inferior vena cava (IVC) junction with the atrium, accounts for 10% to 15% of ASD in adulthood. Sinus venosus ASD is frequently associated with anomalous drainage of one or more pulmonary veins usually into the right atrium or SVC. The least common type of ASD is the unroofed coronary sinus with direct communication between the coronary sinus and the left atrium resulting in a left-to-right shunt.

In the situation of a previously undiagnosed ASD in the adult, an echocardiogram is typically ordered to evaluate symptoms of dyspnea, effort intolerance, atrial arrhythmias, or even neurologic symptoms suspicious for an embolic event. Indirect echocardiographic evidence of enlargement and volume overload of the right ventricle may first raise the possibility of a significant left-to-right shunt from an ASD and was one of the first characteristics of ASD described on M-mode and 2D echocardiogram.[26–31] In addition to findings of dilation of the right ventricle, the interventricular septum will be noted to move paradoxically (Fig. 11.1). Motion of the interventricular septum is dependent on the relative pressures of the right and left ventricles during systole and diastole. In right ventricular volume overload due to significant left-to-right shunting through an ASD, the relative pressures in the ventricles equalize in diastole, resulting in characteristic diastolic flattening of the septum. The left ventricular

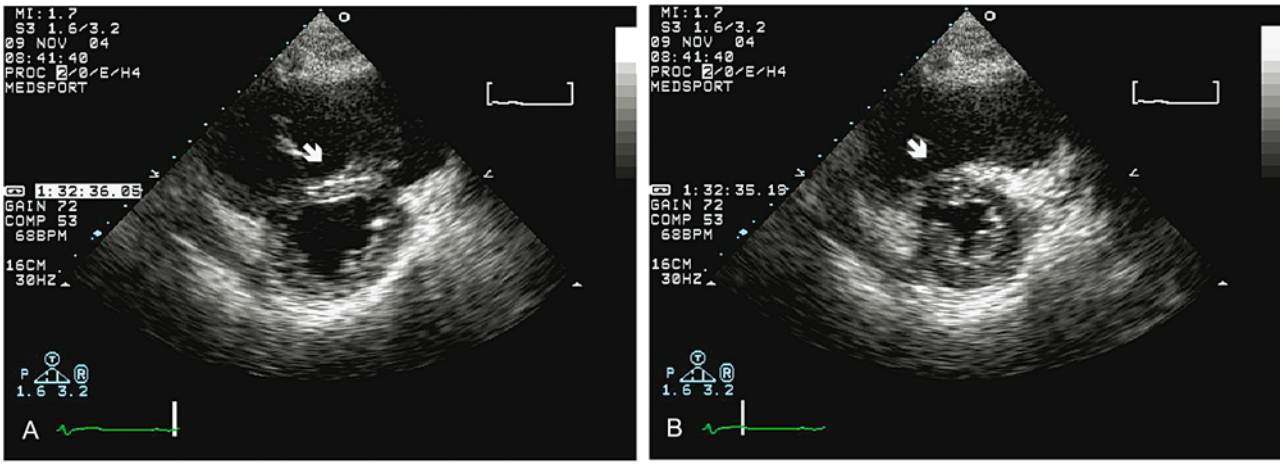

FIGURE 11.1. (A,B) Parasternal short axis view of the ventricles demonstrating paradoxical septal motion of right ventricular volume overload. In diastole (A), right ventricular pressure equals left ventricular pressure, the interventricular septum is flat (arrow), and the left ventricle is D-shaped. In systole (B), left ventricular pressure is greater than right ventricular pressure and the ventricle resumes its normal circular geometry.

cavity assumes a D-shape in diastole as viewed from parasternal short axis view of the 2D echocardiogram. In systole, left ventricular pressure exceeds right ventricular pressure (the normal hemodynamic state) and the interventricular septum resumes its normal circular geometry. In patients with ASD and pulmonary hypertension, right ventricular pressure will equal left ventricular pressure throughout the cardiac cycle and the ventricular septum will remain flattened in both diastole and systole, referred to as a right ventricular pressure overload appearance.[32,33] In children with ASD, 2D and spectral Doppler have been used to quantitate the pulmonary to systemic blood flow ratio (Qp/Qs) with fairly good correlation with that determined by cardiac catheterization.[34,35] However, in adults, correlation between echocardiographic methods of shunt quantification and catheterization is poor; echocardiographic shunt quantification is not of practical use in adults.[36]

Most ostium secundum and ostium primum ASDs are accurately diagnosed with the combination of transthoracic 2D and Doppler echocardiography. In one study, ASD was accurately diagnosed and categorized as primum, secundum, or sinus venosus in 47 of 50 adults using 2D and color Doppler imaging. Three of five sinus venosus defects proven at surgery were missed on TTE.[36] The presence of a secundum ASD may be suggested on the apical four-chamber view by abrupt dropout of echoes in the area of the fossa ovalis with bright side lobe artifacts producing an inverted T-shape.[37] Because the interatrial septum is parallel to the ultrasound beam when the transducer is in the apical position, attenuation of the ultrasound beam and the relative thinness of the membranous part of the septum compared to the muscular portion may result in a false-positive diagnosis of secundum ASD by 2D TTE. The appearance of a color flow signal from the left to right atrium in the apical view can assist in the diagnosis of secundum defects. Transesophageal echocardiography is excellent for localizing the defect (Fig. 11.2). When the ultrasound transducer is in the subcostal location with a transverse imaging plane, the interatrial septum is perpendicular

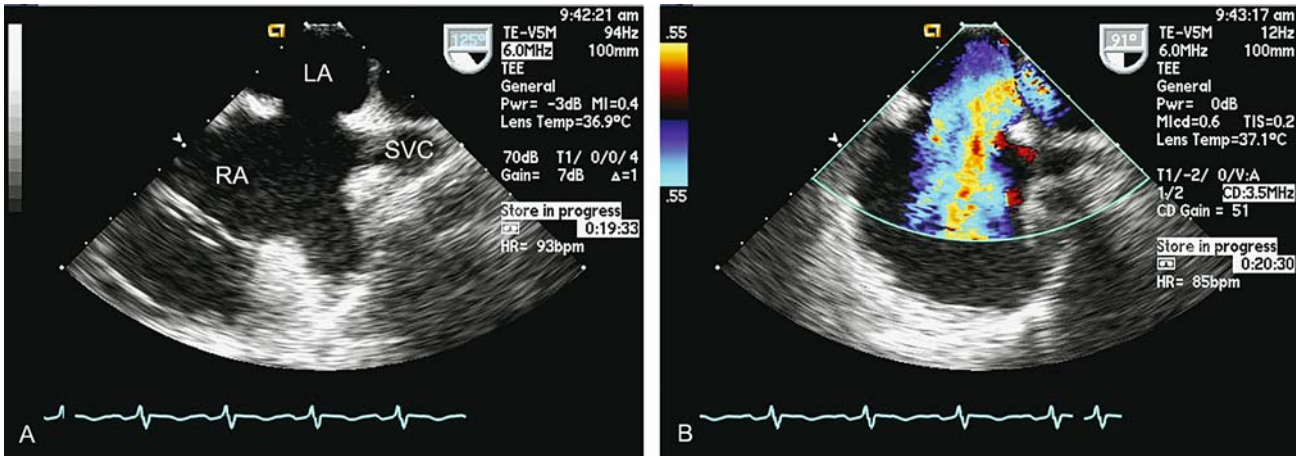

FIGURE 11.2. (A,B) Transesophageal echocardiogram of an ostium secundum atrial septal defect (ASD) in the long axis plane. The defect is in the region of the fossa ovalis with a rim of superior limbus tissue between the superior vena cava (SVC) and the defect (A). Color Doppler flow imaging (B) shows a large left-to-right shunt. LA, left atrium; RA, right atrium.

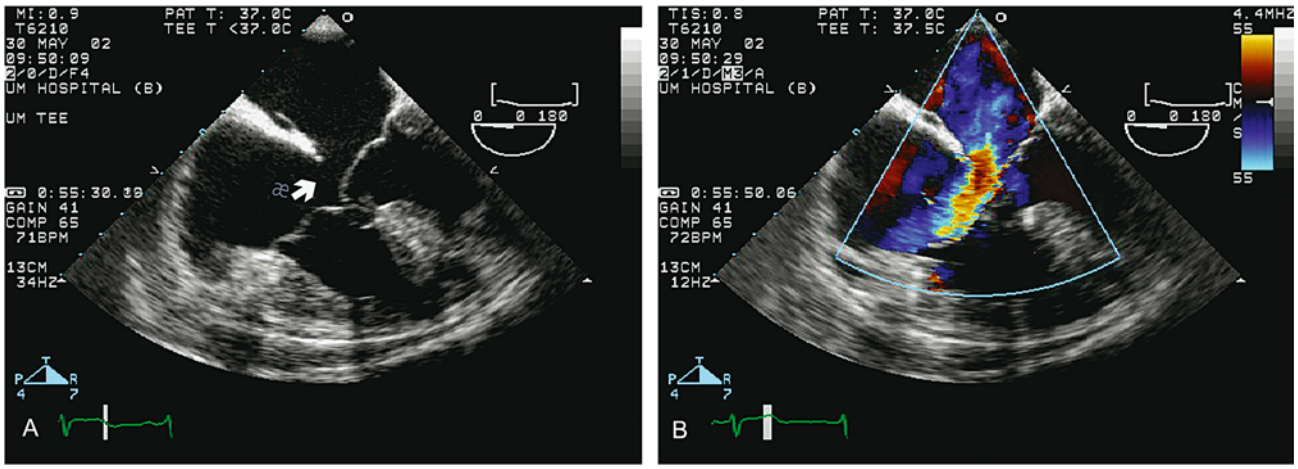

FIGURE 11.3. (A,B) Transesophageal echocardiogram of an ostium primum ASD. The defect is seen at the junction of the interatrial septum and ventricular septum at the level of the atrioventricular (AV) valves (A, arrow). Shunting is primarily left-to-right on color Doppler with a zone of flow convergence seen on the left atrial side of the septum (B).

to the beam of the ultrasound and ASDs may be viewed more directly. In 154 adults with documented ASD in whom adequate subcostal views could be obtained, 89% of secundum, 100% of primum, and 44% of sinus venosus defects were successfully visualized.[38] Ostium primum defects are easily identified on TTE in either the apical four-chamber or subcostal views and on TEE as echo dropout in the lower portion of the interatrial septum at the level of the AV valves (Fig. 11.3). When a primum ASD is recognized, a cleft in the anterior leaflet of the mitral valve may be seen on the parasternal short axis view of the ventricle at valve level, and eccentric mitral regurgitation is almost always present on color Doppler imaging (Fig. 11.4). It is not unusual to visualize a small aneurysm of the inlet portion of the interventricular septum beneath the tricuspid valve that may be formed when some of the septal leaflet of the valve has sealed over a ventricular septal defect that was originally part of the endocardial cushion defect.

Sinus venosus ASDs are frequently missed on 2D TTE and color Doppler because of the posterior location of the defect and the distance of the defect from the ultrasound beam; if seen at all, they are best visualized from the subcostal view in adults. The existence of a sinus venosus ASD is often suggested when no definite secundum or primum ASD is seen on 2D or color Doppler but right ventricular enlargement with right ventricular volume overload motion of the interventricular septum is present. The appearance of microbubbles in the left atrium shortly after the appearance of bubbles in the right atrium subsequent to injection of agitated saline into a peripheral vein further suggests the diagnosis.

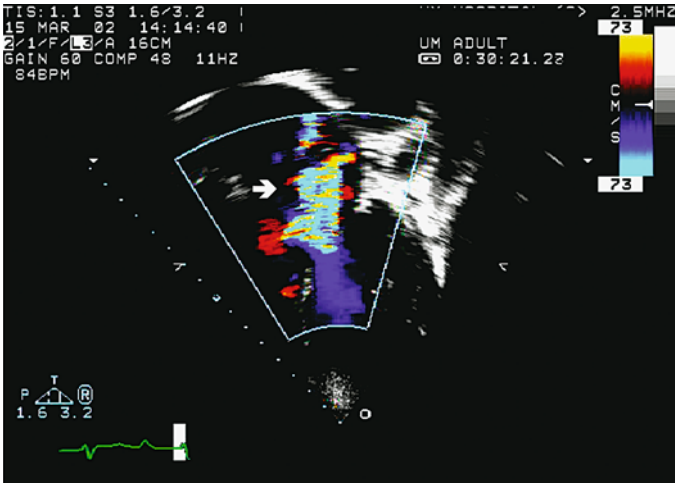

FIGURE 11.4. Color jet of mitral regurgitation in the left atrium on apical four-chamber view in a patient with ostium primum ASD.

Saline contrast injections can be used to diagnose all forms of ASD. A "positive" saline contrast study with appearance of bubbles in the left atrium, however, documents only the existence of a right-to-left shunt which could result from intracardiac shunts other than ASD, including pulmonary arteriovenous malformations or systemic to pulmonary artery collaterals. The appearance of bubbles in the left atrium occurring six or more cardiac cycles after appearance in the right atrium should suggest an intrapulmonary right-to-left shunt. The sensitivity of saline contrast study for the diagnosis of ASD or PFO can be increased by asking the patient to perform a Valsalva maneuver to transiently increase right-sided intracardiac pressures and increase the shunt during the contrast injection.[39–42] More specific for the diagnosis of atrial septal defect is a "negative contrast" study in which a "clear space" appears in the microbubble opacification of the right atrium due to left-to-right shunting of unopacified blood across the ASD (Fig. 11.5).[43] False-positive "negative contrast" effects can occur in the absence of ASD due to unopacified blood flowing into the right atrium from the inferior vena cava, coronary sinus, or anomalous pulmonary veins. Both PFO and atrial septal aneurysm (Fig. 11.6) with PFO can be associated with right-to-left or left-to-right shunting on contrast study. For the diagnosis of right-to-left shunt through a patent foramen ovale or atrial septal aneurysm and the detection of a source of cardiac embolus in patients with unexplained cerebral ischemia, TEE is superior to TTE.[44–52]

Because of its close proximity to the interatrial septum and obviation of most acoustic impediments, TEE generates high-resolution images and is ideally suited for the diagnosis

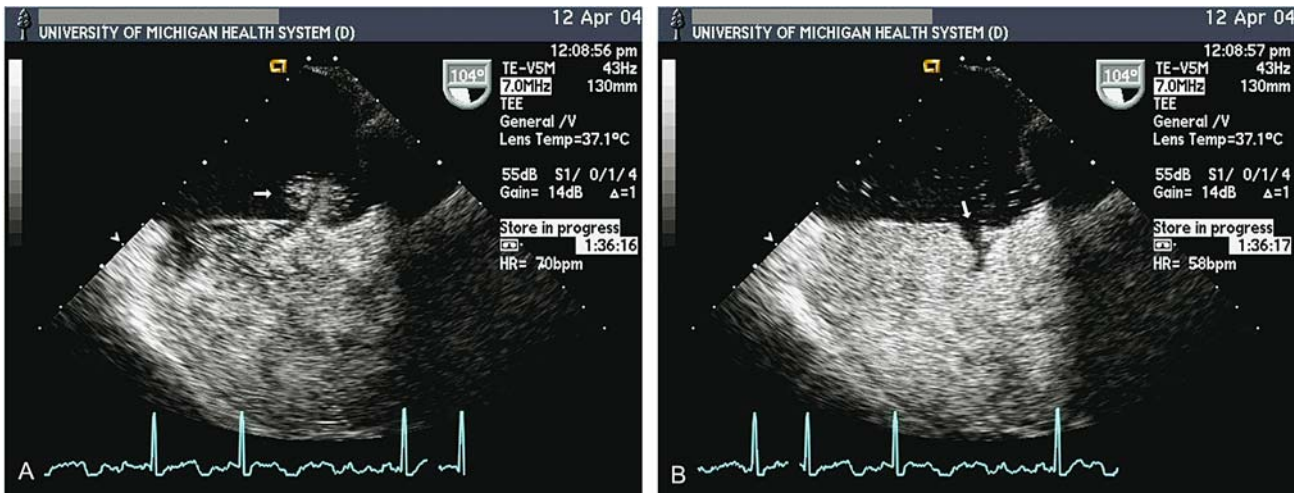

FIGURE 11.5. (A,B) Saline contrast injection in a patient with ostium secundum ASD. (A) Microbubbles are seen crossing the interatrial septum from the right into the left atrium (arrow). (B) A negative contrast effect is demonstrated when unopacified blood from the left atrium passes into the right atrium (arrow), creating an echocardiographic "clear space."

and characterization of ASD. In studies of patients with known secundum ASD, TEE was superior to TTE for the diagnosis of ASD.[53] Defect size measured by TEE showed good correlation with defect size found at surgery.[54] Because TEE provides complete characterization of the interatrial septum, it is the diagnostic procedure of choice for visualizing sinus venosus ASD to both the SVC (Fig. 11.7) and the IVC (Fig. 11.8).[55] The longitudinal esophageal plane is the most useful for diagnosis of sinus venosus ASD on TEE. In a study of 25 adults with sinus venosus ASD on TEE, only three patients had defects that were clearly defined by TTE, though another 11 had venosus ASD suspected on the basis of color flow mapping, while another 10 adults were evaluated to find the cause of unexplained right-heart enlargement on TTE. The importance of TEE in these patients was further emphasized by the finding of 37 anomalous pulmonary veins preoperatively in 23 of 25 patients, requiring alterations in operative approach.[56] In the most common form of partial anomalous pulmonary venous return, the right upper pulmonary vein is seen entering the atrium at the junction of the sinus venosus defect and the SVC with color flow directed into the right atrium, but one or more pulmonary veins may drain into the SVC directly, into the IVC, or into a hepatic vein. Every attempt should be made to identify all pulmonary venous connections in the patient undergoing TEE for ASD. Occasionally, anomalous pulmonary veins occur in patients with secundum ASD, so these should be sought in all patients with secundum ASD. In the rare patient with the unroofed coronary sinus defect, TEE may image the connection between the coronary sinus and the left atrium, and left-to-right shunt may be seen on color flow mapping.

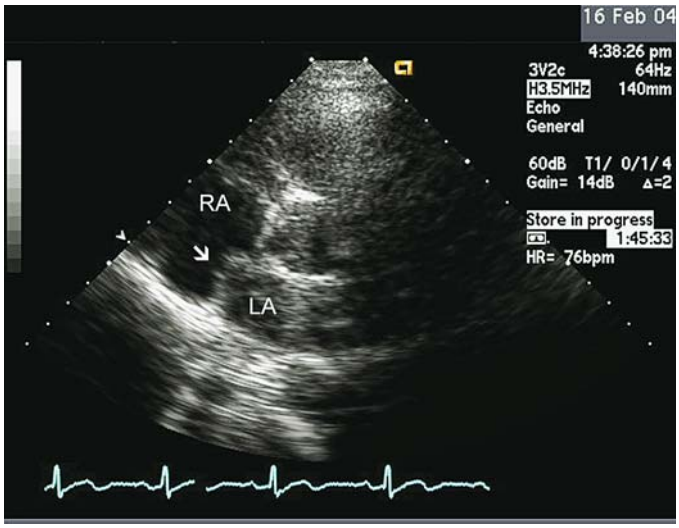

FIGURE 11.6. Atrial septal aneurysm. In the parasternal short axis view, a bulging of the interatrial septum with displacement of the septum into the right atrium is noted (arrow). A displacement of 1 cm into either atrium is the typical criterion for the diagnosis of ASA. The ASA may demonstrate mobility with the respiratory cycle. RA, right atrium; LA, left atrium.

Like patients with ostium secundum and ostium primum ASD, patients with sinus venosus ASD do not require routine preoperative cardiac catheterization if pulmonary hypertension is not demonstrated.[57,58] For adults with suspected secundum ASD, TEE provides significant useful information if transcatheter closure of the ASD is being considered.[59] With appropriate experience, the size of the ASD on TEE can be used to assist in device size selection.[60] Closure devices for ASD require that an adequate "rim" of septal tissue be present on all edges of the defect to ensure adequate seating of the device. This can be quantified by TEE or by intracardiac echocardiography. Three-dimensional reconstruction of TEE images of the interatrial septum may provide additional information to the interventional cardiologist for device selection and assessment of deployment.[61] Also, TEE can identify multiple defects for which additional closure devices might be necessary and identify anomalous pulmonary venous drainage, which might necessitate a surgical rather than transcatheter approach. Recently, intracardiac echocardiography has been used in the catheterization laboratory to monitor percutaneous closure of ASD or PFO and may be less expensive than TEE with equivalent success.[62–64] On echocardiography, the ASD occluder device appears as linear bright echoes on either side of the interatrial septum (Fig. 11.9) and should be examined for security of its seating on

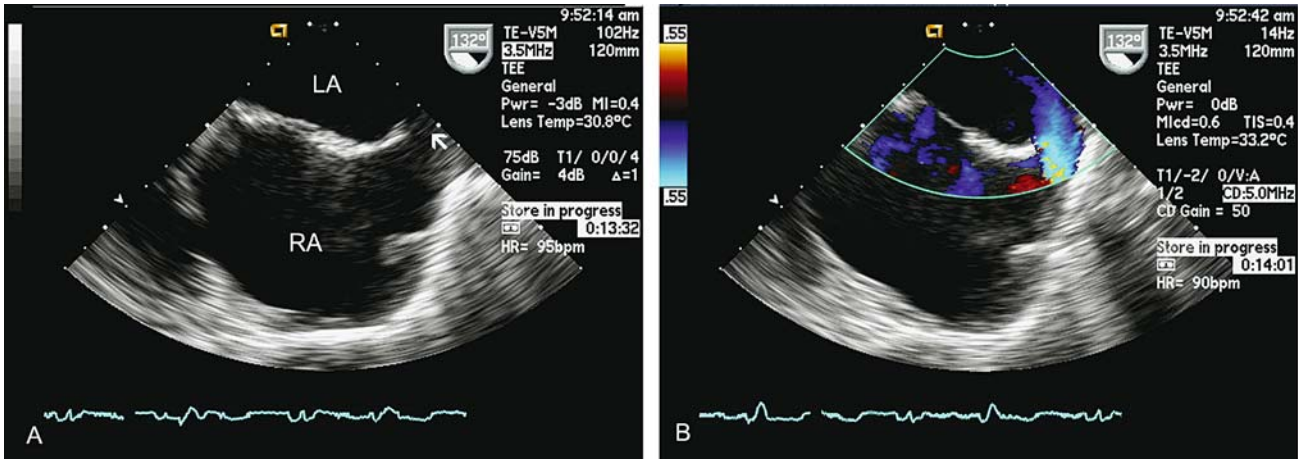

FIGURE 11.7. (A,B) Sinus venosus ASD to the superior vena cava on transesophageal echocardiography (TEE) in the long axis view. The defect is visualized in the most superior portion of the septum (arrow) immediately beneath the superior vena cava (A). Color Doppler shows the left-to-right shunt (B). LA, left atrium; RA, right atrium.

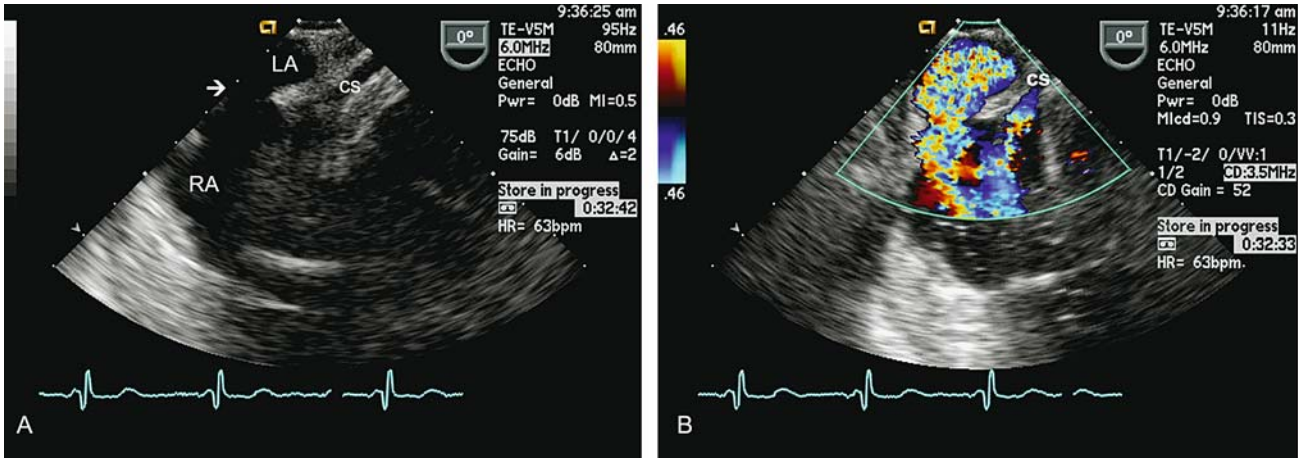

FIGURE 11.8. (A,B) Sinus venosus ASD to inferior vena cava. The defect (arrow) is seen in the inferior portion of the septum adjacent to the coronary sinus (cs) in (A) with large left-to-right shunt demonstrated in (B). RA, right atrium; LA, left atrium.

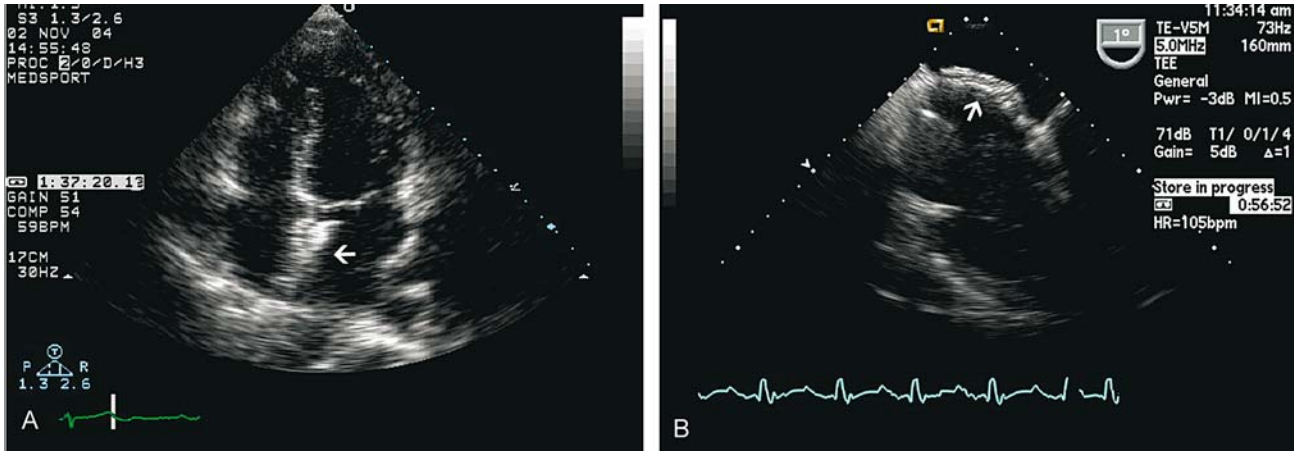

FIGURE 11.9. (A,B) An ASD septal occluder device seated on the interatrial septum. The device is seen as parallel linear echoes on either side of the septum (arrow) on the apical four-chamber view of TTE (A) and TEE (B).

the septum and residual shunt on color Doppler flow mapping. Although the frequency of serial follow-up in adults with corrected ASD has not been established, these patients may develop late atrial arrhythmias or pulmonary hypertension and require continued monitoring.

Ventricular Septal Defect

The most common congenital cardiac defect diagnosed in childhood, VSD is much less commonly diagnosed in adults, in large part because 60% of small VSDs close spontaneously before the teenage years. The remainder of VSDs have already been repaired by adulthood or are large and associated with fixed pulmonary vascular disease, absence of murmur, reversal of the intracardiac shunt (Eisenmenger's syndrome), and cyanosis. A more common scenario is the adult with a loud murmur and small, hemodynamically insignificant VSD. Rarely, an adult may present with a moderately sized VSD and symptoms of heart failure. Because small VSDs confer a significant risk of endocarditis and larger VSDs are associated with a much higher risk of pulmonary hypertension than ASDs, the echocardiographic recognition of VSD is essential for these patients.

Defects of the ventricular septum are classified by anatomic location as viewed from the right septal surface. The most common type of VSD, making up 70% of all VSDs, occurs in the membranous septum often with involvement of adjacent muscular tissue beneath the crista supraventricularis when viewed from the right ventricle and under the aortic valve when viewed from the left. This defect is more properly termed a perimembranous VSD but is also called a subaortic VSD and is a type of outlet VSD. Defects in the muscular portion of the septum are the next most common accounting for 20% of VSD and may occur anywhere in the septum from inlet to trabecular to outlet. Muscular VSDs may be multiple in which case they are termed *Swiss-cheese* defects and are the most difficult to identify echocardiographically. Defects located beneath the pulmonic valve, another form of outlet VSD, are referred to as supracristal, doubly committed, or subpulmonic VSDs and represent approximately 5% of all VSD. Because supracristal VSDs undermine the aortic annulus, prolapse of an aortic cusp can occur with the development of aortic insufficiency, which, if more than mild, constitutes an indication for closure of even small supracristal VSDs. Rarely occurring in isolation, defects of the inlet septum occur beneath the septal leaflet of the tricuspid valve and are often accompanied by defects of the primum portion of the atrial septum as part of an AV septal or endocardial cushion defect also known as an AV canal.

Because of the complex, curved shape of the ventricular septum, multiple transducer locations and imaging planes with both 2D and color and spectral Doppler must be used to interrogate the entire septum. The sensitivity and specificity of echocardiography for the diagnosis of VSD are related to the size and location of the defect. The best views of a particular defect occur when the defect is perpendicular to the ultrasound beam. Because a significant length of septum is perpendicular to the ultrasound plane and axial resolution is best when the transducer is the subcostal location, subcostal views may be helpful, especially in thin adults.[65] The hallmark of VSD on 2D echocardiography is echo dropout of the ventricular septum. The finding of a T-sign in the apical views increases the specificity for the diagnosis of VSD in the same fashion as for ASD.[66–69] Frequently, the VSD is not well visualized on 2D imaging, but high-velocity turbulent flow in systole on color Doppler provides a definitive diagnosis.[70]

Surface TTE is approximately 80% to 90% sensitive for the diagnosis of perimembranous VSD. Perimembranous defects are best visualized in the parasternal long axis and parasternal short axis views. In the parasternal long axis view, the defect appears immediately below the aortic valve. In small, restrictive perimembranous VSDs, a turbulent systolic jet passes from the left ventricular outflow tract into the right ventricle through the defect (Fig. 11.10). It is important to remember that large VSDs with equalization of right and left ventricular pressure may be seen as a sizable defect with no turbulent systolic flow on color Doppler. In the parasternal short axis view at the level of the aortic valve, the turbulent jet is seen to the left of midline near the insertion of the tricuspid valve at the 10 o'clock position if the

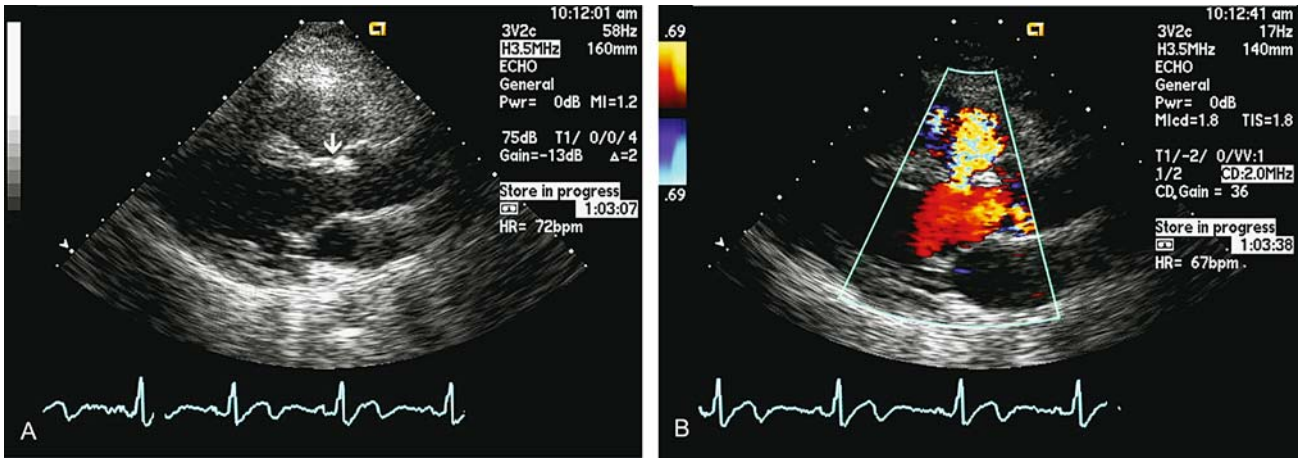

FIGURE 11.10. (A,B) Perimembranous VSD. The defect in the region of the membranous interventricular septum is not well seen on the parasternal long axis view of the TTE (A, arrow). It is characterized by turbulent flow from the left to the right ventricle on color flow Doppler (B).

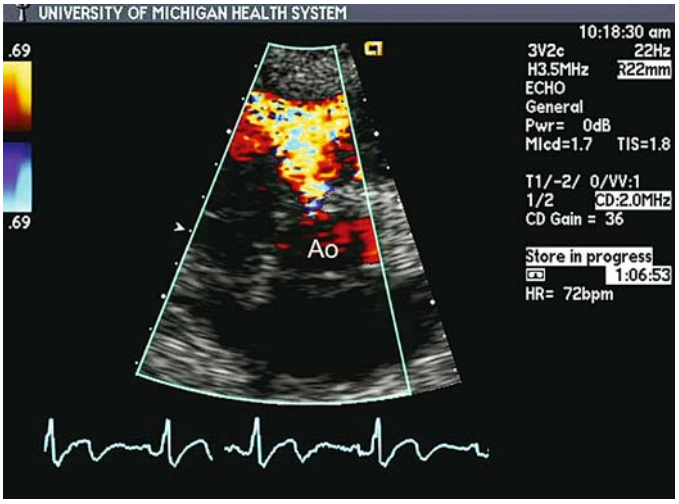

FIGURE 11.11. Color Doppler in the parasternal short axis view showing a turbulent jet immediately inferior to the tricuspid valve seen at approximately the 10 o'clock position on the clock face of the aortic valve (Ao).

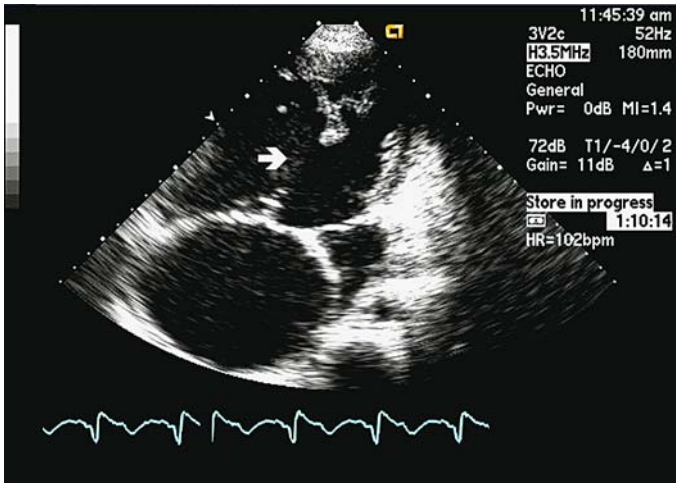

FIGURE 11.12. Large inlet VSD. The defect in the interventricular septum (arrow) is seen in the superior septum at the crux of the heart in the apical four-chamber view.

aortic valve is considered to be a clock face (Fig. 11.11). Supracristal VSDs are also best seen in the parasternal short axis view at the base of the heart and appear as a systolic color flow jet just beneath the pulmonic valve at the 2 o'clock position on the aortic valve. Small supracristal VSDs may be missed, especially if careful color Doppler imaging is not performed. The highest sensitivity of echocardiography in VSD is for inlet defects, which are best seen in the apical four-chamber view (Fig. 11.12). For uncomplicated inlet VSD without an atrial component, the septal leaflet of the tricuspid valve originates from its normal apically displaced position relative to the mitral valve. In AV canal-type defects, both AV valves are in the same plane and their chordal attachments must be determined.

On occasion, the septal leaflet of the tricuspid valve may partially close an inlet VSD, and a rare type of communication between the left ventricle and the right atrium called a Gerbode defect may result.[71] Muscular VSDs, when small, are the most difficult to identify on TTE, with sensitivity as low as 50% for their detection. Color Doppler must be performed of the entire expanse of the ventricular septum in multiple views including parasternal long axis, parasternal short axis from apex to base, subcostal long and short axes, and apical views if a muscular VSD is suspected. Some muscular VSDs appear as narrow channels in the ventricular septum with openings into the left and right ventricles at different levels on the septum (Fig. 11.13). In adults, it is not uncommon to find a ventricular septal aneurysm in the region of the membranous septum, which appears as a thin membrane that bulges into the right ventricle, rarely causing right ventricular outflow tract obstruction, and may incorporate a portion of the septal leaflet of the tricuspid valve.[72] The septal leaflet can completely or only partially seal the perimembranous defect, and this can be best visualized by color Doppler in the parasternal long axis view (Fig. 11.14).

Although 2D and color Doppler can identify the presence and estimate the size of VSDs, continuous wave spectral Doppler accurately quantitates the pressure gradient between the left and right ventricles. By measuring systemic pressure with a blood pressure cuff and subtracting the pressure gradient between the left and right ventricle, the right ventricular systolic pressure can be estimated. In the absence of pulmo-

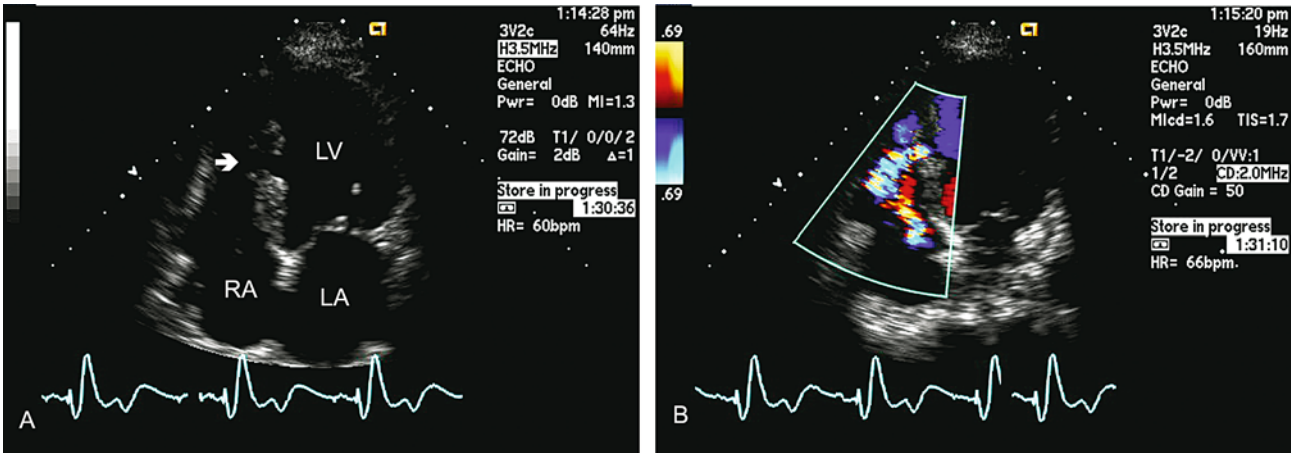

FIGURE 11.13. (A,B) Muscular VSD in the midportion of the trabecular septum (arrow) in the apical four-chamber view (A) with high-velocity color jet from left to right (B). LV, left ventricle; LA, left atrium; RA, right atrium.

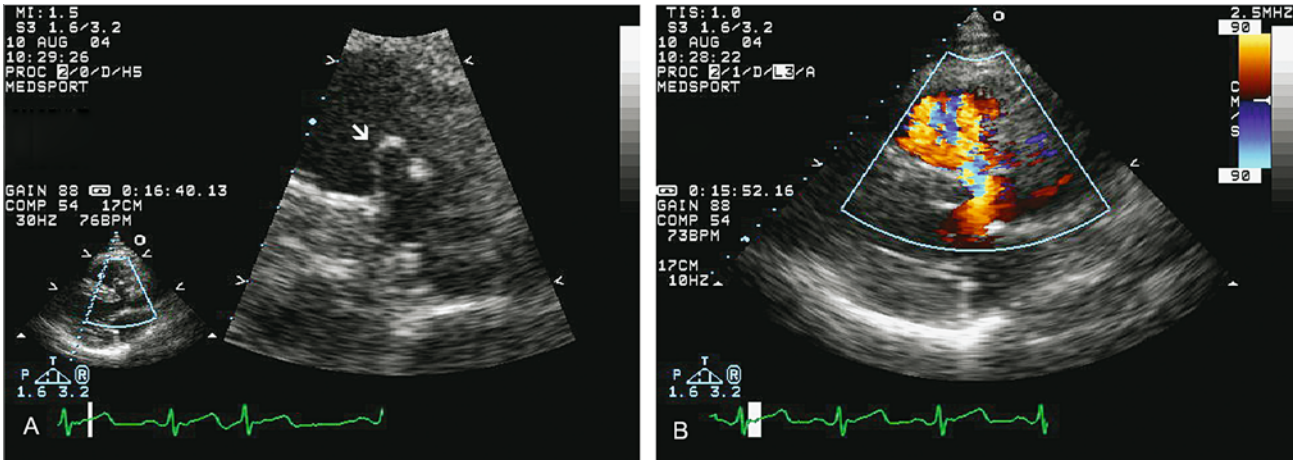

FIGURE 11.14. Parasternal long axis view of ventricular septal aneurysm. Parts of the septal leaflet of the tricuspid valve partially seal over a perimembranous VSD. This is seen as a localized bulge of the membranous septum (arrow) into the right ventricle (A). Color Doppler flow confirms the VSD (B).

nary outflow obstruction, the pulmonary systolic pressure can be inferred from the right ventricular systolic pressure. With careful alignment of the Doppler cursor with the turbulent jet on color flow imaging, the peak velocity of the VSD jet can be measured (Fig. 11.15). Using the modified Bernoulli equation in the usual fashion,

$$\text{Peak gradient} = 4 \times V^2 \text{ (peak velocity squared)}$$

the peak gradient between the ventricles is calculated.[73–75] Small restrictive VSDs will have high gradients, often in excess of 100 mm Hg, whereas large, nonrestrictive VSDs have low or no gradients, reflecting the fixed pulmonary hypertension that is present in most adults with the defect.

The normal postoperative appearance of the septum after surgical closure is typified by a bright linear echo on the right ventricular side of the defect if a prosthetic patch was used.[76] Dehiscence of the patch may be visualized from multiple views by a turbulent systolic jet on color Doppler at the margin of the patch (Fig. 11.16) or mobility of the echodense patch into the right ventricle in systole.[77] Echocardiography

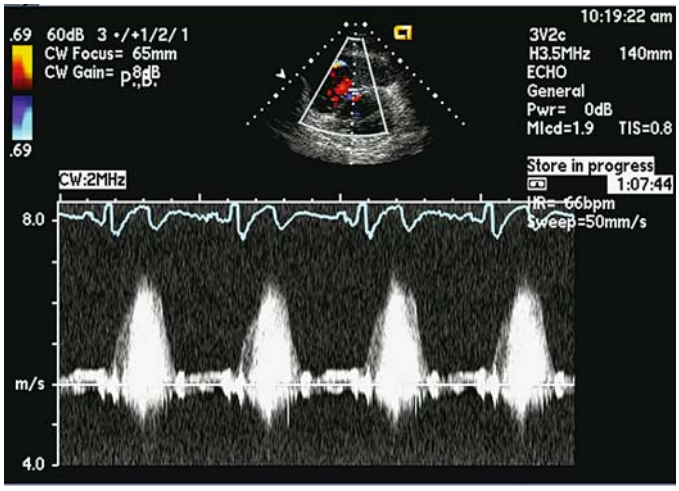

FIGURE 11.15. Continuous wave Doppler of restrictive perimembranous VSD with peak velocity approximately 5.6 m/sec. The peak pressure gradient between the left and right ventricle is calculated to be 125 mm Hg by the modified Bernoulli equation.

is integral to the assessment of other complications of VSD including evaluation of aortic insufficiency in patients with supracristal VSD who have prolapse of a (usually right) coronary cusp into the defect,[78] pulmonary hypertension, or endocarditis with vegetation[79] typically of right heart structures at the site of jet impingement. Infrequently, an adult may present who underwent banding of the pulmonary artery (PA) in childhood to protect from fixed pulmonary vascular disease, but never proceeded to closure of the defect. An example of a PA band in an adult patient with a nonrestrictive VSD and pulmonary hypertension is shown in Figure 11.17. By measuring the systemic blood pressure by cuff and subtracting the sum of the peak gradient across the VSD and the peak gradient across the PA band, PA systolic pressure can be estimated. A recent development is the closure of perimembranous and muscular VSDs using transcatheter closure devices.[80,81]

Atrioventricular Septal Defects (Atrioventricular Canal or Endocardial Cushion Defect)

Atrioventricular septal defects occur due to failure of fusion of the inferior and superior endocardial cushions to varying degrees, with abnormalities of the AV junction ranging from isolated primum ASD with cleft mitral valve (MV) and isolated inlet VSD ("partial" AV canal with separate AV valves) to complete AV canal with a spectrum of abnormalities of the AV valves. Echocardiography with color Doppler can readily determine the size and extent of the septal defects, the nature of the shunt, and the morphology of the AV valves.[82] The extent of the atrial and ventricular components of the defect is best gauged in the apical four-chamber or subcostal views. In these views, the nature of the AV valve(s) and attachments should be carefully explored. Some patients may have a single (common) AV valve (Fig. 11.18). In the patient with two AV valves in the same plane, chordal attachments of the valves must be elucidated. The presence of a straddling AV valve with chordal attachments crossing the septal defect to insert into the opposite ventricle makes the surgical repair more complex than does an overriding valve that overlies the AV septal defect but has no chordal attachment to the

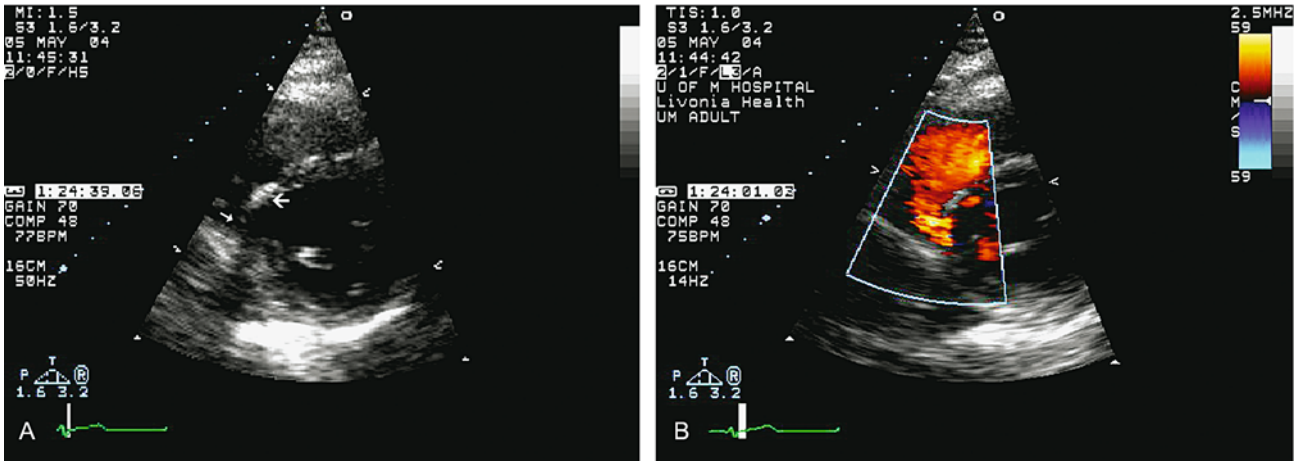

FIGURE 11.16. (A,B) Prosthetic VSD patch dehiscence. In the parasternal short axis view, a bright linear echo is seen on the right ventricular side of the inferior septum (large arrow) with associated echo dropout of the defect (small arrow) (A). Flow across the defect is seen on color Doppler (B).

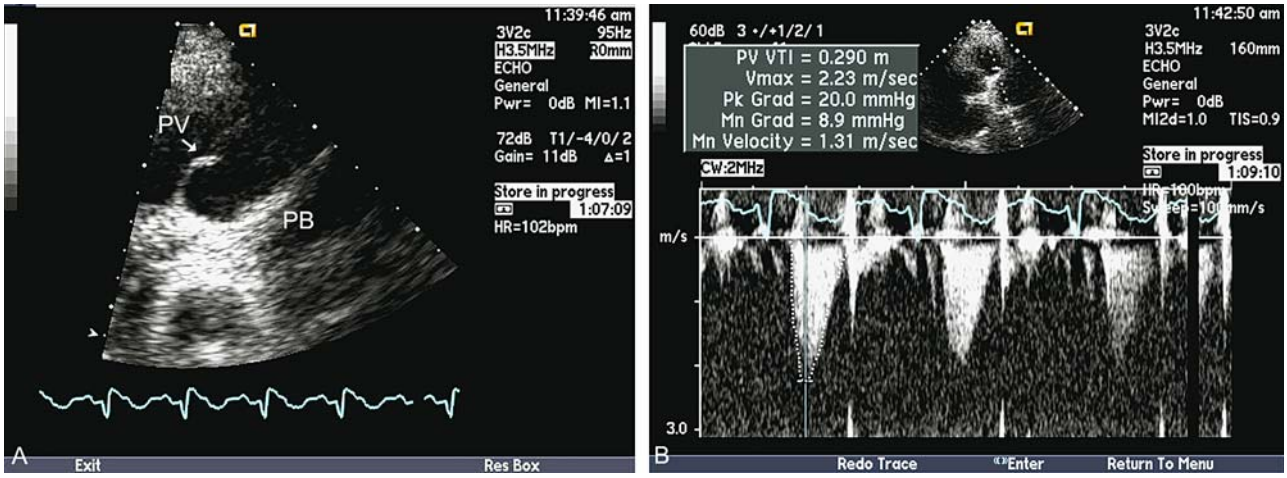

FIGURE 11.17. (A,B) In the high parasternal view, there is a band noted on the main pulmonary artery (arrow) just distal to the pulmonic valve (A). The peak gradient across the pulmonary artery band (B) is 20 mm Hg, suggesting that there is insufficient protection of the distal pulmonary vascular bed from increased pulmonary blood flow through the ventricular septal defect.

FIGURE 11.18. (A,B) Atrioventricular septal defect (AV canal or endocardial cushion defect). In the apical four-chamber view, a large defect involving the superior portion of the atrial septum (top large arrow) and the inferior portion of the ventricular septum (bottom large arrow) is seen (A). The common AV valve is seen in diastole (small arrows) in A and in systole (large arrow) in B.

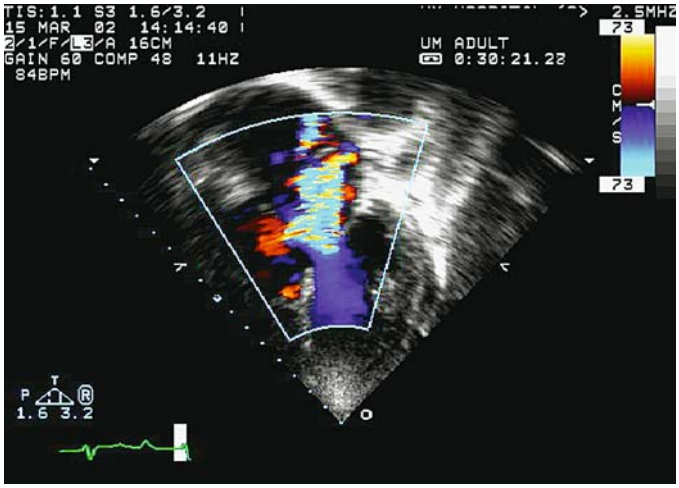

FIGURE 11.19. Color Doppler flow image of regurgitation of the AV valve in a patient with AV septal defect.

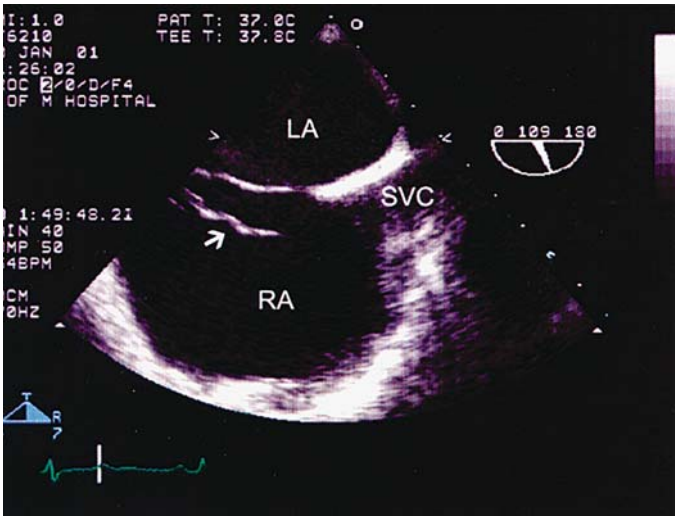

FIGURE 11.21. Transesophageal echocardiogram of complete eustachian valve. The eustachian valve is the flap valve of the inferior vena cava (arrow). SVC, superior vena cava; RA, right atrium; LA, left atrium.

opposite ventricle. In patients with a primum ASD, the associated cleft anterior mitral valve leaflet is best directly visualized in the parasternal short axis view, though the eccentric mitral regurgitation may be appreciated in the apical views. Although most patients present after having been repaired in childhood, some adults, particularly patients with Down syndrome who were not operated, present with pulmonary hypertension and cyanosis. Atrioventricular valve regurgitation (Fig. 11.19) is common in these patients.

Abnormalities of Venous Inflow

The most frequent congenital anomaly of systemic venous inflow is persistence of a left SVC, which is found in approximately 0.5% of the general population and up to 10% of patients with other congenital heart defects. Embryologic resorption of the right-sided SVC in utero is rare in these patients, and an absent right SVC was seen in only three of 10 patients evaluated by magnetic resonance imaging.[83] The left SVC usually drains directly into the coronary sinus and then to the right atrium with no physiologic consequences, but on rare occasion will drain into the left atrium or pulmonary vein. Most often, a persistent left SVC is suspected when a dilated coronary sinus that appears as a large circular structure in the posterior AV groove is noted on the parasternal long axis view of the TTE. Persistence of the left SVC is the most common cause of a dilated coronary sinus on TTE. The coronary sinus can also be visualized with steep posterior angulation in the apical four-chamber view as a longitudinal structure behind the left atrium draining into the right atrium. In adults, the actual left SVC is not often directly visualized. Instead, the diagnosis is clinched by injection of agitated saline into a peripheral vein in the left arm. In this instance, bubbles will first be seen in the coronary sinus followed by opacification of the right heart (Fig. 11.20).[84–87] Injection of agitated saline into a vein in the right arm produces direct opacification of the right heart without opacification of the coronary sinus. Although not an abnormality, a prominent or "complete" eustachian valve at the junction of the inferior cava extending to a varied degree to the ostium of the coronary sinus warrants mention (Fig. 11.21) because

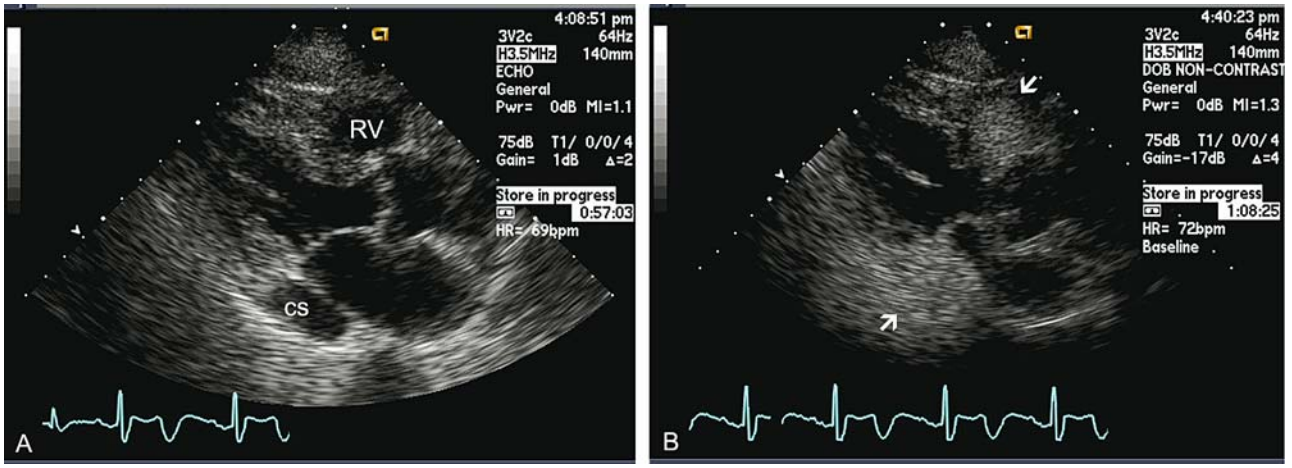

FIGURE 11.20. (A,B) Persistent left superior vena cava. In the parasternal long axis view, a dilated coronary sinus (cs) is seen posterior to the left atrium in the AV groove (A). When agitated saline is injected in a peripheral vein in the left arm, bubbles appear first in the coronary sinus and then the right atrium and ventricle (B, arrows). RV, right ventricle.

it can cause confusion and misdiagnosis as thrombus or vegetation.

Anomalous pulmonary venous drainage in adults is most frequently seen in association with a sinus venosus defect, but may be an isolated abnormality with one or more pulmonary veins draining into the SVC, IVC, right atrium, or hepatic vein. Unrepaired total anomalous pulmonary venous return is not seen in adults. In adults with normal pulmonary vein anatomy, the right superior, and left superior and inferior pulmonary veins may be identified draining into the left atrium in the apical four-chamber view. The right inferior pulmonary vein is not visualized in adults on TTE. Often the only clue to the presence of isolated anomalous pulmonary veins is enlargement of the right heart with no right-to-left shunt on saline contrast injection. Preoperative identification of abnormal pulmonary vein drainage in patients with ASD is important for defining the approach to these patients since a procedure to baffle flow from the vein to the left atrium will be necessary in addition to repair of the defect. For these patients, TEE is more accurate than TTE for the diagnosis of anomalous pulmonary veins.[88–92] Congenital stenosis of pulmonary veins is not seen in the adult population. However, TEE has proved useful for arrhythmia mapping in the pulmonary veins during radiofrequency ablation of atrial fibrillation and diagnosing pulmonary vein stenosis that can occur as a late complication of the procedure.[93,94]

Abnormalities of Ventricular Inflow

The most common anomalies involving the inflow tract of the right ventricle are tricuspid atresia or hypoplasia and Ebstein's anomaly. Patients with tricuspid atresia have an obligate intraatrial communication and usually have associated hypoplasia of the right ventricle. Because these patients are generally managed as patients with single ventricle physiology, they will be considered in the section on single ventricles.

Ebstein's anomaly, an abnormality of tricuspid valve development, is characterized by apical displacement of the insertion of the septal (and sometimes posterior) leaflet of the tricuspid valve and variable elongation of the anterior leaflet, designated a "sail" leaflet owing to its resemblance to the sail of a ship. There is a wide spectrum of tethering of the anterior leaflet to the ventricle by multiple abnormal short chords. This abnormality results in apical displacement of the tricuspid valve coaptation point into the right ventricle with "atrialization" of the inlet portion of the right ventricle as a consequence. Ebstein's anomaly, often accompanied by a secundum ASD or PFO, most often presents in childhood with signs of right heart failure or cyanosis and has a less favorable prognosis in this population. In many instances, however, Ebstein's does not present until adulthood, even in patients with severe apical displacement of the tricuspid valve. In one study of 72 adults diagnosed with Ebstein's anomaly, the mean age at first diagnosis was 24 years.[95] In general, suitability for tricuspid valve repair versus replacement is determined by valve morphology, and prognosis is related to the size of the functional right ventricle.

The tricuspid valve morphology, chordal attachments, and functional right ventricular size can be accurately assessed using multiple views on TTE.[96,97] The degree of apical displacement of the septal leaflet is best estimated from the apical four-chamber view. Because some degree of apical displacement of the septal leaflet is present in the normal heart and may be accentuated by right ventricular enlargement from any cause, echocardiographic criteria have been developed to make the diagnosis of Ebstein's anomaly in adults. In one study, an absolute value of 20-mm displacement of the septal tricuspid leaflet relative to the insertion point of the anterior leaflet of the mitral valve was used. In other studies, a distance of 8 mm/m^2 when normalized to body surface area provided an accurate diagnosis of Ebstein's.[98] Tethering of the anterior leaflet should be evaluated in the apical four-chamber view (Fig. 11.22). Assessment of tethering of the anterior leaflet and functional right ventricular size may also be performed in the right ventricular "inflow" view obtained by anterior and medial angulation of the ultrasound beam from a left parasternal long axis transducer position. A functional right ventricle area smaller than 35% of the total ventricle and extensive tethering of the anterior leaflet portend a less favorable surgical outcome.[97] In unoperated adults with Ebstein's, the septal leaflet attachment ratio, defined as the distance from the AV valve annulus to the distal attachment of the septal leaflet divided by the total ventricular septal length in the four-chamber view at end diastole, did not correlate with the percent of atrialized area of the right ventricle. However, a higher index (indicating more severe apical displacement) was associated with worse prognosis for survival.[95] Both TTE[97] and TEE[99] can be used to assess suitability for and adequacy of tricuspid valve reconstruction. In Ebstein's anomaly, there is usually severe tricuspid regurgitation with the origin of the color Doppler jet occurring at the coaptation point of the tricuspid valve, close to the right ventricle apex (Fig. 11.23).

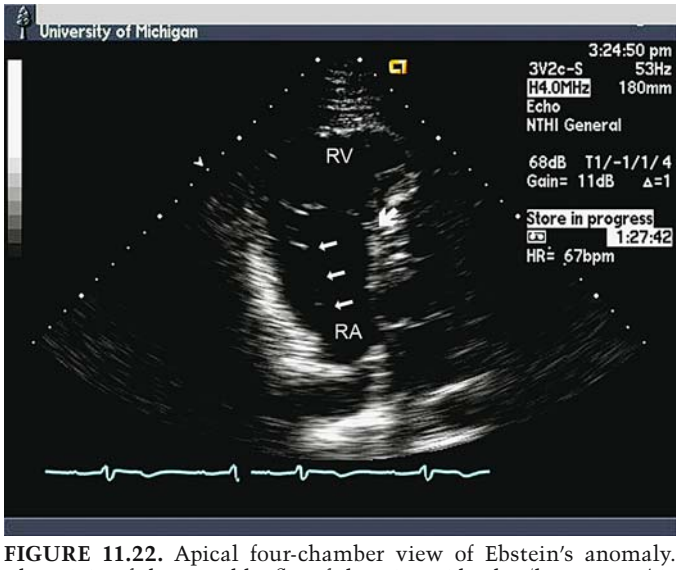

FIGURE 11.22. Apical four-chamber view of Ebstein's anomaly. The origin of the septal leaflet of the tricuspid valve (large arrow) is displaced toward the right ventricle (RV) apex. The anterior "sail leaflet" (small arrows) is elongated with multiple chordal attachments to the anterior wall of the RV. There is a large area of atrialized RV superior to the valve. RA, right atrium.

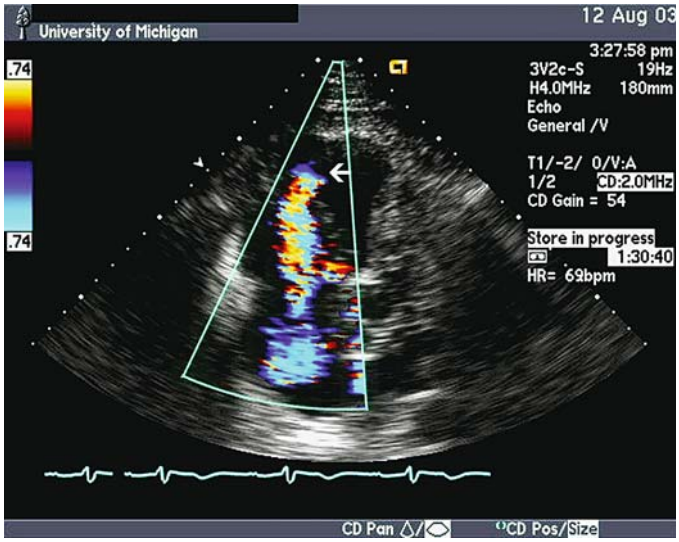

FIGURE 11.23. Color Doppler flow image of Ebstein's anomaly in the apical four-chamber view. The origin of the jet of tricuspid regurgitation (arrow) is displaced far toward the right ventricular apex.

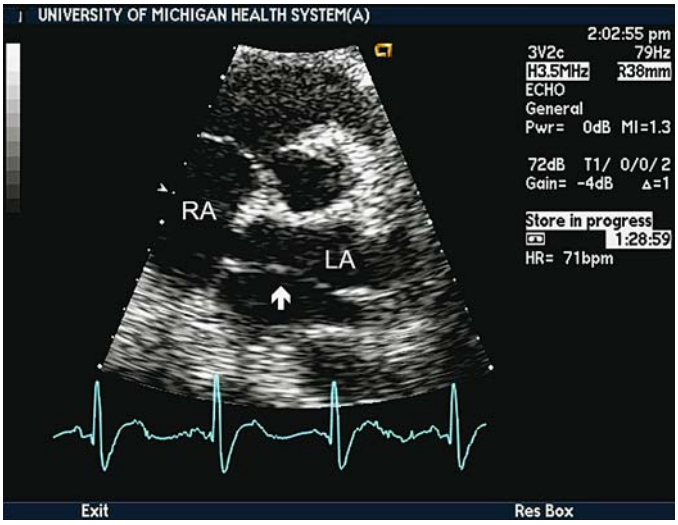

FIGURE 11.24. Parasternal short axis view of the left atrium showing the membrane of cor triatriatum (arrow). RA, right atrium; LA, left atrium.

Obstruction to inflow of the left ventricle can take the form of cor triatriatum, mitral supravalvular ring, congenital mitral stenosis, or mitral atresia (usually as part of complex left ventricular inflow and outflow obstructive lesions known as Shone complex). Shone complex is always diagnosed in infancy and childhood and therefore will not be dealt with here.

Cor triatriatum, caused embryologically by incomplete resorption of the floor of the common pulmonary vein as it merges with the roof of the left atrium, is characterized by the presence of a perforated membrane that divides the left atrium into a superior chamber that receives the pulmonary veins and an inferior chamber associated with the left atrial appendage and the mitral valve. In most instances, the opening in the membrane is restrictive. Patients present with symptoms of left ventricular inflow obstruction with pulmonary congestion. Asymptomatic adults with cor triatriatum first identified as an incidental finding on TTE may have a nonrestrictive membrane. Cor triatriatum is usually readily identified on TTE.[100,101] The membrane is often identified on TTE in the parasternal views where it is seen in the left atrium inserting anteriorly at the level of the posterior wall of the aorta and coursing to the posterior left atrial wall (Fig. 11.24). However, the membrane is best visualized on TTE in the apical view in the middle left atrium since it is perpendicular to the ultrasound beam (Fig. 11.25). The left atrial appendage may be identified in the lower chamber. Pulmonary veins can be visualized draining into the superior chamber and may be dilated if obstruction of the fenestration is significant.

The site of obstruction in the membrane can be identified by a turbulent color flow jet in the middle atrium that is primarily diastolic, but can persist throughout the cardiac cycle if stenosis is severe. The transmembrane gradient can be calculated (reflecting severity of stenosis of the orifice) using the modified Bernoulli equation from the peak velocity obtained by pulsed or continuous wave Doppler in the apical views.[102] If the diagnosis is suggested but not clear on TTE, TEE can provide clear images of the membrane, its attachment to the interatrial septum and lateral wall of the atrium above the atrial appendage, and the nature of the opening,[103] thus guiding operative resection.[103–106] A stenotic supravalvular mitral ring differs from cor triatriatum in that it occurs at the level of or slightly superior to the mitral annulus, is sometimes adherent to the base of the valve leaflets, but is below the left atrial appendage. Small rings may be difficult to image with 2D echocardiography, but may be suggested if color Doppler demonstrates turbulent inflow to the left ventricle above the mitral valve leaflets. The echocardiogram of a patient with a supravalvular ring is shown in Figure 11.26.

Congenital mitral stenosis, usually diagnosed in childhood, may be difficult to differentiate from rheumatic mitral stenosis on echocardiogram in adults. Congenital mitral

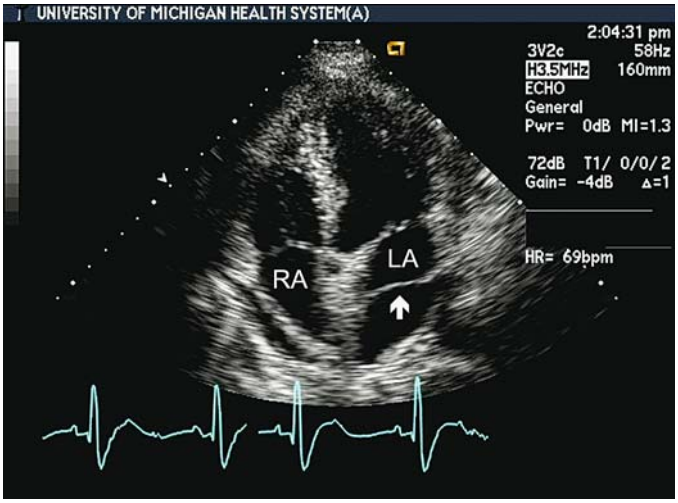

FIGURE 11.25. The membrane of cor triatriatum (arrow) is seen coursing across the left atrium (LA) in the apical four-chamber view.

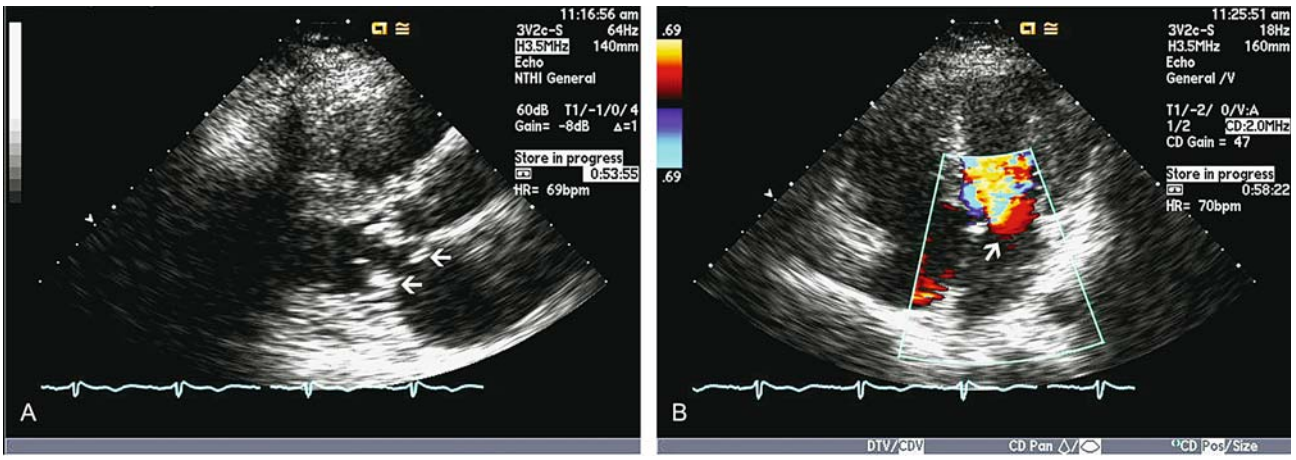

FIGURE 11.26. (A,B) A supravalvular mitral ring is noted just superior to the mitral valve at the mitral annulus in A (two arrows) in the parasternal long axis view. On color Doppler flow imaging in the apical four-chamber view (B), the convergence zone for mitral inflow is above the level of the mitral valve signifying obstruction at that level.

stenosis is usually the result of abnormal insertion of chordae tendineae into either a single papillary muscle, the "parachute" type of mitral valve, or into multiple small papillary muscles, the "arcade" type. Both types of congenitally stenotic valves can be visualized in apical and short axis views of the ventricle on TTE. An occasional adult will exhibit a "double orifice" mitral valve, which has the hallmark of two separate orifices seen on short axis cross-sectional views of the ventricle at valve level. The degree of stenosis of these valves is variable and dependent on insertion of the chords (usually each orifice inserts into its own papillary muscle making this, technically, a double parachute mitral valve) and chordal fusion.[107–109]

Abnormalities of Ventricular Number or Morphology

Single Ventricle Complexes

Many different congenital abnormalities may result in what is physiologically a single pumping chamber in which oxygenated and deoxygenated blood mix before being pumped to the body. In single ventricle hearts, a small outlet chamber may exist with communication from the main ventricle through a defect known as a bulboventricular foramen. The rudimentary chamber does not have an inlet and is technically not a ventricle. Echocardiography permits extensive evaluation of the wide spectrum of congenital abnormalities resulting in a single ventricle.[110] Often, the univentricular heart can be classified morphologically as right, left, or indeterminate by its appearance on 2D TTE. The most common type of univentricular heart is the morphologic left ventricle and is referred to as a double-inlet left ventricle. Double-inlet right ventricles also exist. If the single ventricle is a left ventricle, a rudimentary outlet chamber with connection to a pulmonary artery should be sought anterior and superior to the ventricle. The rudimentary chamber in a morphologically right single ventricle is posterior and inferior to the ventricle. Patency of the bulboventricular foramen can be assessed on color Doppler flow imaging. Multiple complex abnormalities are common in these patients. Ventriculoarterial discordance with the aorta arising from the anterior outlet chamber and the pulmonary artery arising from the posterior chamber is especially common.

Tricuspid atresia results from failure of development of the tricuspid valve. At birth, an ASD or PFO must be present for survival. There is usually significant underdevelopment or hypoplasia of the right ventricle with mixing of oxygenated and deoxygenated blood in the left ventricle causing cyanosis. Although the small right-sided chamber receives the inlet of the tricuspid valve in the form of a fibrous ring, and therefore is technically a ventricle, the physiology is identical to that of other single ventricle complexes.

Patients with this group of defects who survive to adulthood have usually undergone an operation that establishes a connection between the systemic veins or right atrium and the pulmonary arteries to provide pulmonary blood flow and improve oxygenation. In most adults, this connection is created with one of several variations of a Fontan circuit. In one common form of Fontan anastomosis, a connection is made between the right atrial appendage and the PA either by direct anastomosis (Fig. 11.27) or interposition of a conduit. In other individuals, a conduit may be placed from the IVC through the lateral right atrium and connected to the PA, the so-called lateral tunnel Fontan, with connection of the SVC to the PA in a total cavopulmonary connection. Especially in individuals with elevated pulmonary vascular resistance prior to surgery, holes or "fenestrations" may be deliberately placed in the Fontan at the time of surgery to allow the circuit to decompress, but at the cost of increased cyanosis. These fenestrations may be closed using percutaneous interventional techniques at a later time. In other patients, the conduit may be placed from the IVC external to the right atrium to the pulmonary artery, the extracardiac Fontan circuit.

Echocardiography plays a vital role in the understanding and management of patients with univentricular hearts who have undergone the Fontan operation. However, the Fontan connection is often poorly visualized on TTE for many

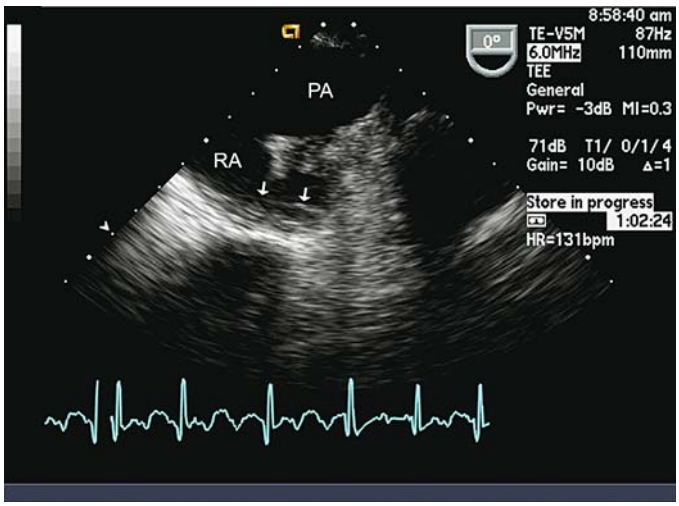

FIGURE 11.27. A classic Fontan anastomosis of the right atrial appendage directly to the pulmonary artery is shown on transesophageal echocardiogram. A layer of thrombus, a common finding after Fontan operation in adults, is noted in the atrium (arrows). RA, right atrium; PA, pulmonary artery.

reasons including multiple prior surgeries and scarring, malposition of the heart in the chest, and the location of most connections behind the sternum. In some adults with direct right atrial anastomosis to the pulmonary artery, the connection may be visualized on high parasternal views on TTE or on TEE. The lateral tunnel Fontan may be seen as a bright circular prosthetic structure within the atrium. The Fontan circuit should also be examined with color Doppler to assess for obstruction and with spectral Doppler to establish flow patterns within the circuit. In patients with low pulmonary vascular resistance, the pattern of flow in the pulmonary artery after Fontan is characterized as biphasic with the largest peak due to atrial contraction in late diastole and a smaller late systolic peak. Flow velocity typically increases during inspiration. In patients with elevated pulmonary vascular resistance or ventricular diastolic pressure, the Doppler pattern may demonstrate a smaller peak in late diastole with reduced respiratory variation, or absence of diastolic flow altogether in extreme cases. Because of low-velocity flow and enlargement of the right atrium, thrombus can develop within the circuit, causing obstruction or pulmonary embolism, especially in adults. Fontan thrombus may be identified on TTE,[111] especially in symptomatic patients. However, TEE is more likely to diagnose thrombus in these patients,[112] an important finding since clinically silent pulmonary embolism has been reported in up to 17% of Fontan patients and anticoagulation is required (Fig. 11.28).[113]

Two congenital abnormalities of ventricular myocardium, arrhythmogenic dysplasia of the right ventricle and isolated noncompaction of the left ventricle, may be first diagnosed in the adult. Arrhythmogenic right ventricular dysplasia (ARVD) is a genetic condition, often with autosomal dominant inheritance, characterized pathologically by fibrofatty replacement of right ventricular myocardium. The patient usually presents with ventricular arrhythmias of left bundle branch block morphology. Since the extent of replacement of ventricular myocardium with fibrofatty tissue is variable, a wide spectrum of echocardiographic abnormalities can be seen, ranging from normal right ventricular size and function, to regional abnormalities with localized "bulging" of the right ventricular free wall, to marked dilation of the entire right ventricle, a condition termed Uhl's anomaly or "parchment" right ventricle. Because the right ventricle has a complex, crescent shape, complete evaluation requires the use of multiple ultrasound planes from subcostal, apical four-chamber, and right ventricular inflow transducer positions. The right ventricle may be incompletely visualized on TTE. The use of echocardiographic contrast agents may improve the sensitivity for the diagnosis of ARVD in these patients.[114] The use of tissue Doppler velocity evaluation may also increase the sensitivity for the diagnosis of early disease.[115]

In isolated noncompaction of the left ventricle, the development of ventricular myocardium is arrested prior to condensation and compaction of the myocardium, and, as a result, some or all of the myocardium has deep trabecular recesses that communicate with the ventricular endocardium. These adults typically present with heart failure or ventricular arrhythmias. Transthoracic echocardiography provides the diagnosis in the majority of patients. On 2D echocardiography, the myocardium appears "spongy" with deep sinusoids (Fig. 11.29). On color Doppler imaging, color may be seen entering the sinusoids. With the use of peripherally injected echocardiographic contrast agents, which may be seen entering the sinusoids, noncompaction can be differentiated from left ventricular thrombus and hypertrophic cardiomyopathy. In one study with pathologic correlation, four echocardiographic criteria were required to be diagnostic for noncompaction: (1) absence of any other cardiac abnormality; (2) echocardiographic appearance of a two-layer structure to the myocardial wall, with a compacted thin epicardial band and a much thicker noncompacted endocardial stripe, and with deep endomyocardial spaces and a maximal end-systolic ratio of noncompacted to compacted layer >2; (3) predominant localization of abnormalities in the midlateral, apical, and mid-inferior regions of the ventricle;

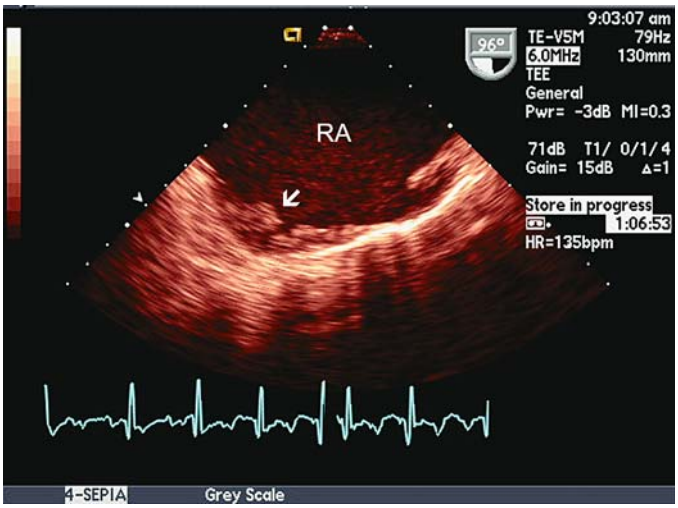

FIGURE 11.28. Transesophageal echocardiogram of right atrial thrombus (arrow) in a patient after Fontan operation. RA, right atrium.

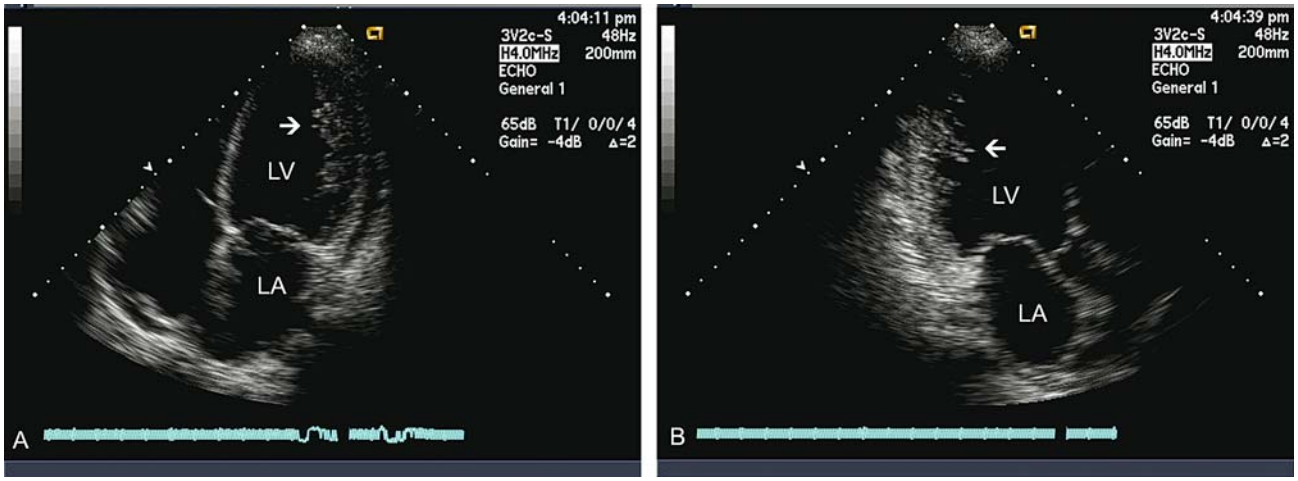

FIGURE 11.29. (A,B) Apical four-chamber (A) and two-chamber (B) views of noncompaction of the left ventricle. Areas of "spongy" appearing myocardium with deep sinusoids are seen in the lateral and inferior walls (arrow) of the left ventricle. LA, left atrium; RA, right atrium.

and (4) color Doppler evidence of deep perfused intertrabecular recesses.[116]

Conotruncal Abnormalities

Tetralogy of Fallot

The most common abnormality of conotruncal development seen in adults is tetralogy of Fallot, a defect consisting of a large subaortic/perimembranous VSD with malalignment of the infundibular septum; anterior and rightward displacement of the aortic root, such that the aortic valve "overrides" the defect; obstruction to right ventricular outflow, which may occur at any level from subvalvular to the branch pulmonary arteries; and right ventricular hypertrophy, resulting from the obstruction. The degree of aortic override from malalignment of the septum correlates with the severity of infundibular stenosis. The VSD with aortic override is the most obvious echocardiographic finding in these patients (Fig. 11.30) and is easily identified in the parasternal long axis view on TTE.[117] Another conotruncal abnormality, the double-outlet right ventricle (DORV), can be confused with tetralogy of Fallot on echocardiography if aortic override is extreme. In DORV, both great arteries arise from the right ventricle, and there is discontinuity between the posterior wall of the aorta and the anterior leaflet of the mitral valve. The diagnosis of DORV is made on TTE if more than 50% of the aorta is seen to override the right ventricle and there is aortic-mitral discontinuity, whereas the appropriate diagnosis is tetralogy of Fallot if more than 50% of the aorta overrides the left ventricle *and* aortic-mitral continuity is preserved.[118,119] Right ventricular outflow obstruction can occur at many levels, which must be evaluated in the patient with tetralogy of Fallot.

Infundibular stenosis due to muscle bundle hypertrophy and anterior displacement of the septum can be visualized in the parasternal and subcostal short axis views at the base of the heart. Valvular stenosis and stenosis of the proximal pulmonary arteries can also be evaluated in this view. Color Doppler may suggest obstruction by the presence of a turbulent jet at the site of the stenosis. Using continuous wave Doppler through the obstruction, the total gradient may be calculated, but obtaining individual gradients at each level obstruction may not be possible. Though most patients with unoperated tetralogy of Fallot have valvular pulmonic stenosis, an infrequent patient may have congenital absence of the pulmonary valve with severe pulmonary insufficiency.[120] In the unoperated young adult who otherwise would not require cardiac catheterization, it is important to identify the origin of the coronary arteries in the parasternal long axis view at the level of the aortic valve.[121] In some patients an aberrant conus branch or left anterior descending artery can be identified crossing the right ventricular outflow tract and could be transected if care is not taken during repair.

Adults with tetralogy of Fallot who present for care have generally been repaired in late childhood or adolescence, though some adults were palliated with a Blalock-Taussig

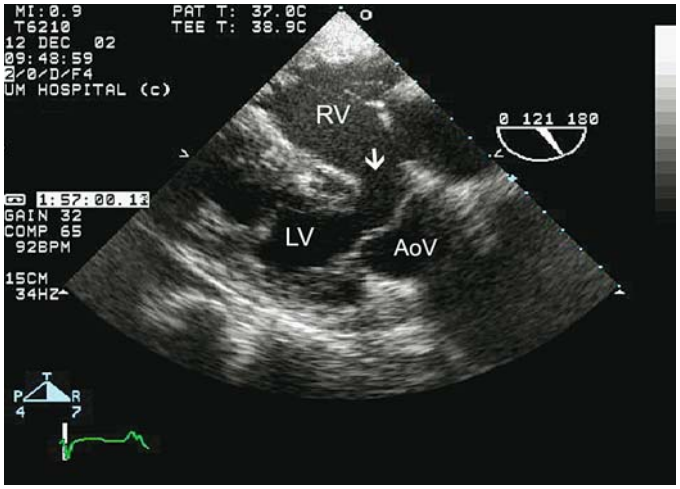

FIGURE 11.30. Parasternal long axis view of tetralogy of Fallot. The aortic valve (AoV) overrides a large, subaortic VSD (arrow). There is marked hypertrophy of the right ventricle (RV). LV, left ventricle.

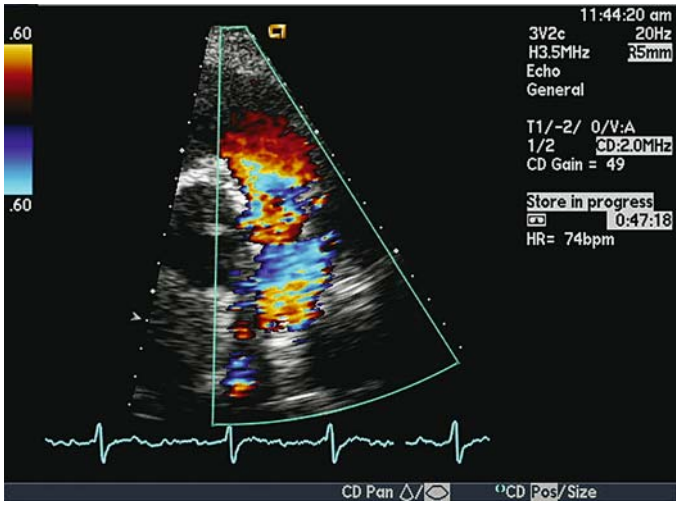

FIGURE 11.31. Color Doppler flow image of the pulmonary valve in the high parasternal short axis view. There is severe pulmonary insufficiency.

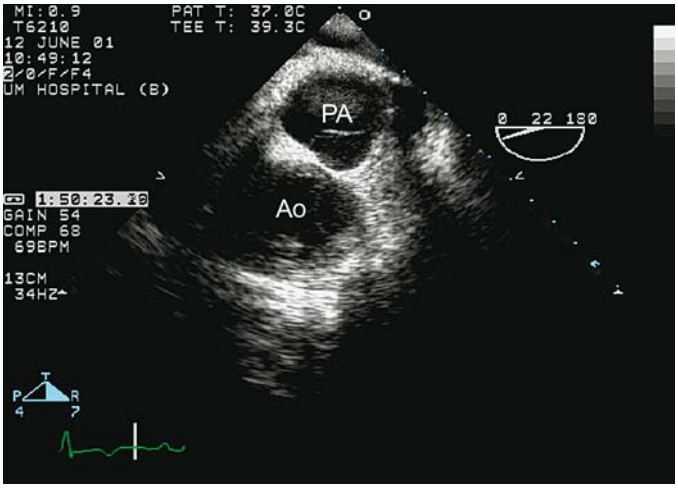

FIGURE 11.32. Transesophageal short axis view of the great vessels in a patient with *d*-transposition of the great arteries. Both semilunar valves appear in short axis. The pulmonary artery (PA) is seen posterior and to the left of the aorta (Ao). In this transesophageal image, the top of the sector corresponds to the transducer location posterior to the heart in the esophagus.

shunt in childhood and never completed the repair. Serial echocardiography is critical to the appropriate management of the postoperative adult with tetralogy of Fallot. Most of these patients, in whom repair included incisions across the pulmonary annulus, many with transannular patches, develop late severe, free-flowing pulmonary regurgitation as a result (Fig. 11.31).[122] Some patients develop aneurysmal dilation of the prosthetic patch, which may be associated with more severe pulmonary regurgitation. Continued volume overload of the right ventricle produces systolic dysfunction that is unlikely to improve if pulmonary valve replacement is delayed until systolic dysfunction is symptomatic.[123] Right ventricular function, though difficult to precisely quantitate echocardiographically, may be easily followed in a serial fashion to monitor for the development of systolic dysfunction. Severe pulmonary insufficiency may beget right ventricular dilation and tricuspid regurgitation, further compromising systolic function.[124] In the patient with severe valvular stenosis or pulmonary atresia who was repaired with a right ventricle to pulmonary conduit, TTE and Doppler may detect valve conduit stenosis due to pannus ingrowth or valve calcification or conduit insufficiency. Echocardiography also detects the sizable subset of adults with tetralogy of Fallot repaired in childhood who now exhibit progressive dilation of the aortic root with aortic regurgitation.[125] Adults who have been repaired uniformly exhibit a right ventricular restrictive diastolic abnormality on spectral Doppler.[126] Interestingly, this restrictive abnormality actually shortens the duration of pulmonary regurgitation and is associated with improved exercise performance in these patients.

D-Transposition of the Great Arteries

In patients with *d*-transposition of the great arteries (*d*-TGA), there is both atrioventricular concordance and ventriculoarterial discordance, with the aorta arising from the anterior right ventricle and the pulmonary artery originating from the posterior left ventricle. The echocardiographic features of the unoperated patient with *d*-TGA were outlined previously and are shown in Figures 11.32 and 11.33. In *d*-TGA, the aorta is usually anterior and to the right of the PA in short axis views. Since the anomaly results in parallel circuits that would not be compatible with life, adult survivors have necessarily undergone operations to restore the normal flow pattern and allow oxygenation of systemic venous blood. In the majority of adults, this procedure consisted of a complete atrial septectomy with placement of either a pericardial or prosthetic baffle in the atrium in the Mustard or Senning operation, also known as the atrial switch procedure. The interatrial baffle is saddle shaped and routes deoxygenated blood from the vena cavae through the mitral valve into the left ventricle and out to the pulmonary arteries. Oxygenated blood returns from the pulmonary veins and is routed superiorly over the baffle through the tricuspid valve to the right ventricle and out the aorta. The interatrial baffle can be

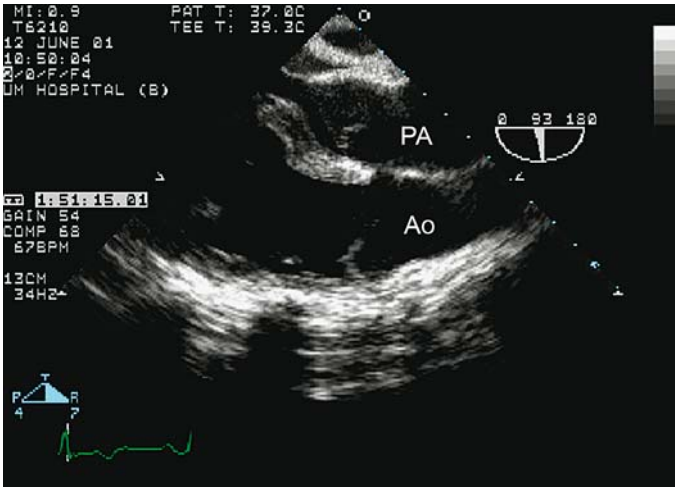

FIGURE 11.33. Transesophageal long axis view of the great vessels in a patient with *d*-transposition of the great arteries. The axes of the pulmonary artery (PA) and aorta (Ao) are parallel rather than orthogonal and the PA is posterior to the Ao.

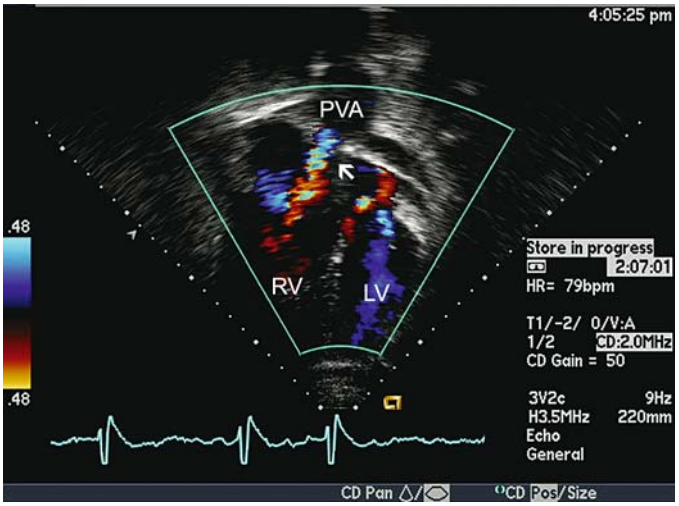

FIGURE 11.34. Apical four-chamber view of a Mustard baffle in a patient with *d*-transposition of the great arteries. Stenosis of the pulmonary venous portion of the baffle is indicated by the narrow color Doppler jet (arrow) from the pulmonary venous atrium (PVA) toward the tricuspid valve. RV, right ventricle; LV, left ventricle.

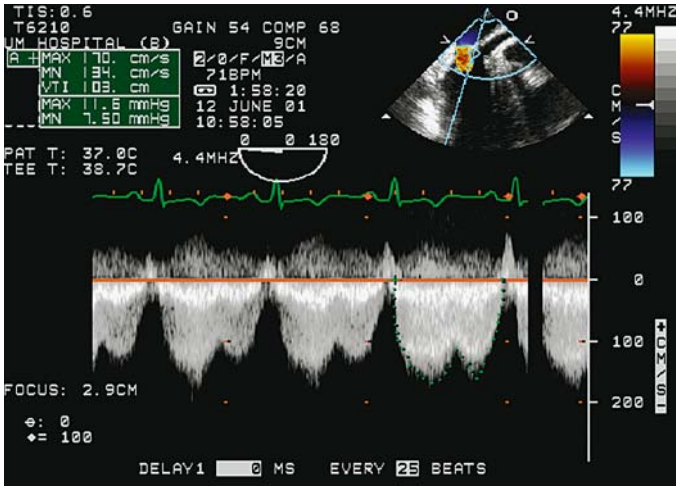

FIGURE 11.35. Continuous-wave Doppler of the stenotic site in the pulmonary venous limb of the Mustard baffle in the patient with *d*-transposition of the great arteries shown in Figures 11.34 and 11.35. The mean gradient across the baffle stenosis is approximately 8 mm Hg.

directly visualized in the parasternal long axis view and in the apical views on TTE as a linear echo within the left atrium, and must be examined along its length for evidence of leak or obstruction.[127] Small leaks of the baffle are common, and, if not seen on color Doppler imaging, may be revealed by peripheral injection of saline contrast. The most common site of baffle obstruction is within the systemic venous limb at the SVC, but is unlikely to be visualized in adults by TTE. Obstruction of the pulmonary venous limb of the baffle may be suspected by a turbulent jet in the baffle on color Doppler or by dilation of the pulmonary veins (Fig. 11.34). The gradient across the obstruction can be estimated from the diastolic velocity obtained with spectral Doppler (Fig. 11.35). In adults in whom acoustic windows and image quality are poor, TEE clearly visualizes all limbs of the baffle (Fig. 11.36). The systemic right ventricle with the usual curvature of the right ventricular septum is seen in Figure 11.37.

Transesophageal echocardiography is also used to monitor transcatheter interventions such as closure of baffle leaks and stenting of SVC obstruction in these patients.[128,129] Most patients with *d*-TGA who have undergone the Mustard operation will exhibit systolic dysfunction of the systemic right ventricle by early adulthood, though most remain asymptomatic until the fourth decade. Transthoracic echocardiography is used to follow systemic ventricular function and monitor for AV valve regurgitation, another fairly common problem in these patients.[130] Patients with *d*-TGA may develop subpulmonic obstruction that can be diagnosed by Doppler. The arterial switch procedure for *d*-TGA involves transection of the great arteries with reanastomosis to the appropriate ventricle and reimplantation of the coronary arteries. The operation restores normal flow direction, with the left ventricle pumping to the systemic circulation and is now the procedure of choice for patients with *d*-TGA. The

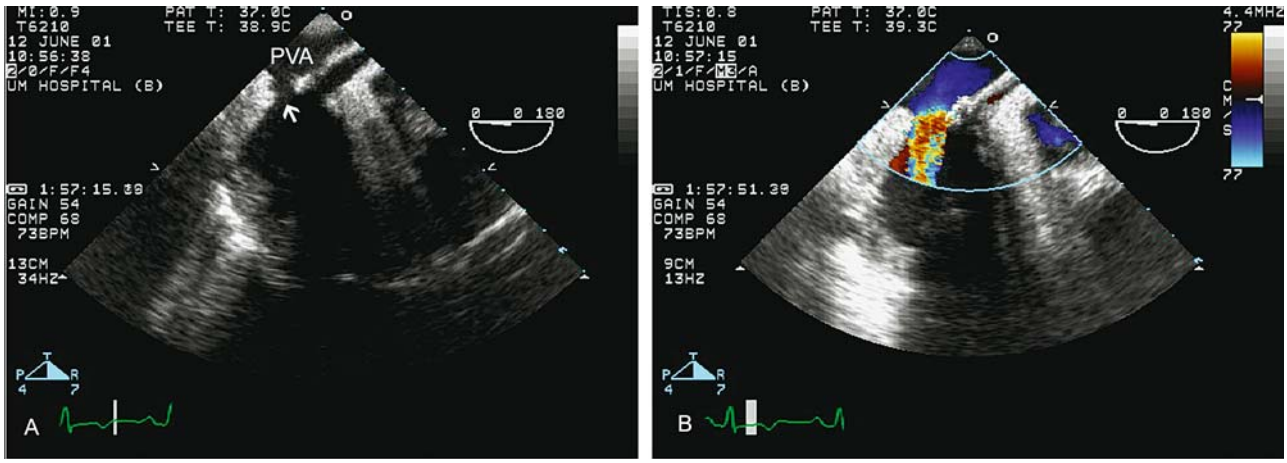

FIGURE 11.36. (A,B) Transesophageal echocardiogram of a Mustard baffle in the same patient with *d*-transposition of the great arteries and obstruction of the pulmonary venous limb of the baffle (arrow, A). A convergence zone is seen on the pulmonary venous atrium side of the baffle consistent with stenosis at that site (B).

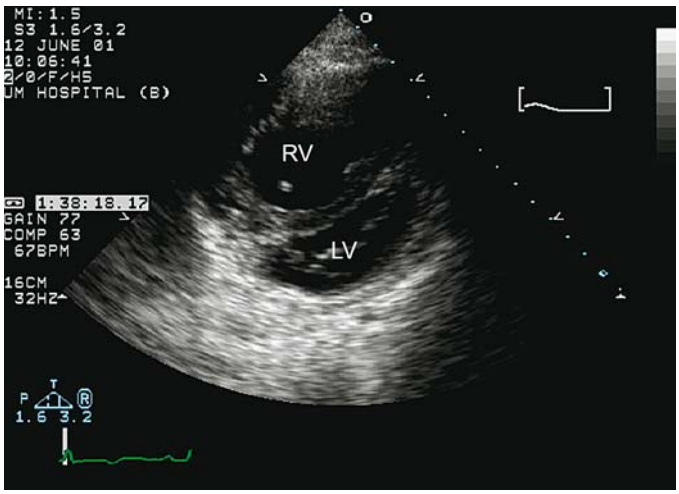

FIGURE 11.37. Parasternal short axis view of the ventricles in an adult with *d*-transposition of the great arteries. The right ventricle (RV) is dilated and the interventricular septum bulges into the left ventricle (LV).

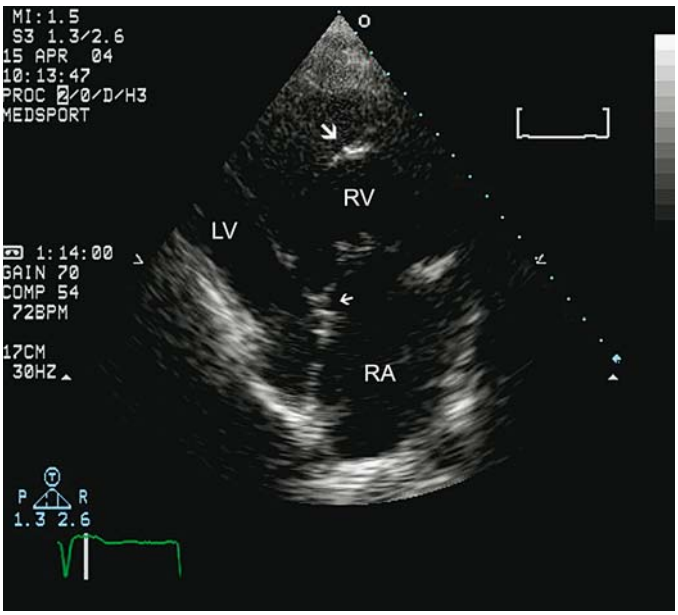

FIGURE 11.38. Apical four-chamber view of a patient with *l*-(congenitally corrected) transposition of the great arteries. The systemic right ventricle (RV) with its moderator band (large arrow) and apically placed septal leaflet of the tricuspid valve (small arrow) is to the left of the left ventricle (LV).

first successful operation was performed in 1975, which means that these patients are now entering their 30s and 40s and require continued echocardiographic monitoring for supravalvular aortic and pulmonic stenosis and left ventricular dysfunction due to ostial stenosis of the coronary buttons.[131]

L-(Congenitally Corrected) Transposition of the Great Arteries

In *l*-transposition of the great arteries (*l*-TGA), the ventricular loop forms to the left and results in inversion and malposition of the ventricles with atrioventricular and ventriculoarterial discordance. As in *d*-TGA, the great vessels exit the ventricles in parallel, but in *l*-TGA the aortic valve is usually anterior and to the left of the pulmonary valve in short axis views at the base rather than to the right of the pulmonary artery. Echocardiographically, the diagnosis is established using multiple views to identify a rightward morphologic left ventricle with smooth endocardium and basally placed mitral valve and a leftward trabeculated right ventricle with an apically displaced tricuspid valve and a moderator band (Fig. 11.38). The great vessel exiting the morphologic left ventricle is seen to course posteriorly and bifurcate into a pulmonary artery while the aorta exits the anterior left-sided right ventricle and extend anteriorly. Adult patients usually have some degree of systolic dysfunction of the systemic right ventricle that should be followed echocardiographically, and most have regurgitation of the left-sided tricuspid AV valve (Fig. 11.39).[132] If a perimembranous VSD, which occurs in 70% of patients with *l*-TGA, is not present, the diagnosis may not be made until adulthood, when systemic AV valve regurgitation and ventricular dysfunction have already supervened. Because systemic AV valve regurgitation is due primarily to morphologic abnormalities of the valve similar to Ebstein's anomaly, operation is more likely to require replacement than repair.

Persistent Truncus Arteriosus

Persistent truncus arteriosus, an abnormality that results from failure of partitioning of the conotruncal region of the heart, is characterized by the presence of a single great vessel positioned over a large outlet VSD (Fig. 11.40). The truncal valve has numerous, up to six, leaflets and, in adults, is almost always regurgitant. Persistent truncus arteriosus is classified by the origin of the pulmonary arteries. The pulmonary arteries may arise as a single vessel from the truncal

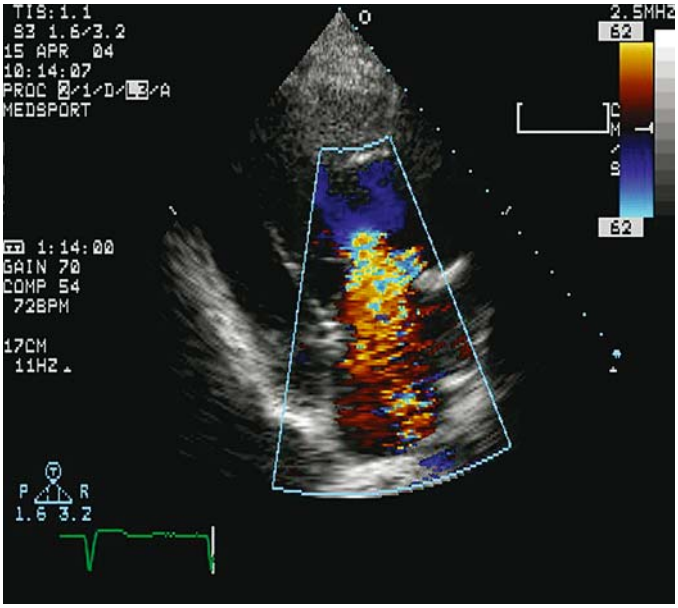

FIGURE 11.39. Color Doppler image in the apical four-chamber view of regurgitation of the systemic (tricuspid) atrioventricular valve in a patient with *l*-(congenitally corrected) transposition of the great arteries.

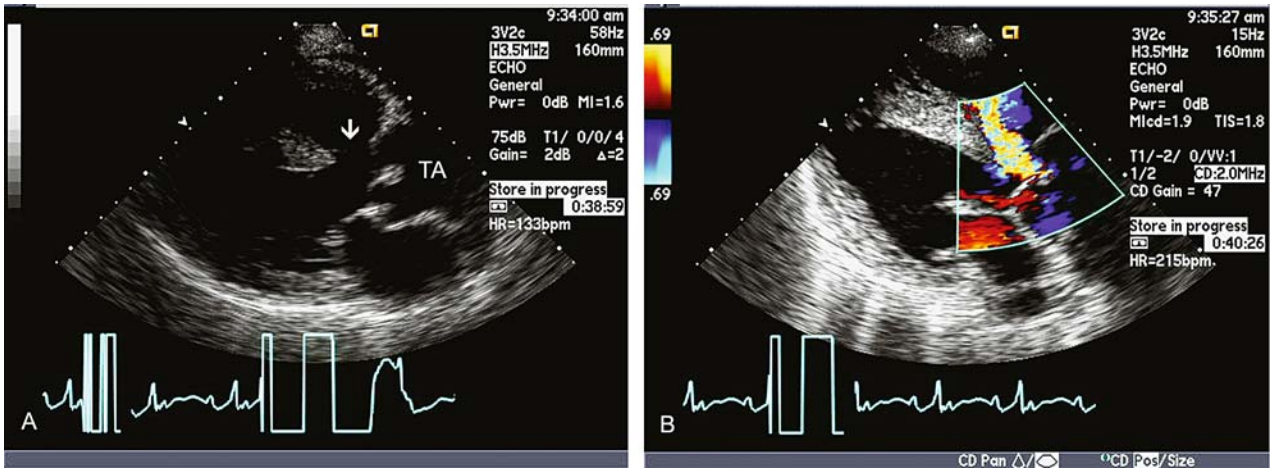

FIGURE 11.40. (A,B) Persistent truncus arteriosus (TA) is seen in the parasternal long axis view (A). There is a single great artery overriding a large outlet VSD (arrow). A jet of truncal valve regurgitation is seen on color Doppler of the truncal valve (B).

artery, which then bifurcates, as separate vessels exiting from the posterior wall, as separate vessels from the sides of the truncus, or discontinuous from the truncus and fed by collaterals from systemic arteries.

Obstruction to Ventricular Outflow

Right Ventricular Outflow Obstruction

Right ventricular outflow tract obstruction can occur at any level including the infundibulum, at the pulmonic valve, or in the pulmonary arteries, all of which can be investigated with 2D and Doppler TTE.[133–137] Obstruction of outflow occurring below the pulmonary valve is a result of a fibromuscular ridge or markedly hypertrophied muscle bundles in the infundibulum, an anomaly known as a double-chambered right ventricle. A double-chambered right ventricle can be difficult to differentiate from severe valvular stenosis with secondary hypertrophy of the muscle bundles. In double-chambered right ventricle, continuous-wave Doppler through the infundibulum will reveal a velocity spectrum characteristic of dynamic obstruction, with the peak velocity occurring in late systole and a dagger-like appearance similar to that seen in hypertrophic obstructive cardiomyopathy involving the left ventricle. Stenosis of the pulmonic valve is characterized by thickening and restricted motion of the tips of the valve leaflets with systolic doming, which is most clearly seen in the parasternal and subcostal short axis views at the base of the heart (Fig. 11.41). The bifurcation of the main pulmonary artery can be identified from a high parasternal transducer location to assess for narrowing of the main pulmonary artery or the branches at their takeoff from the main pulmonary artery. Stenosis of more distal branch pulmonary vessels cannot be visualized echocardiographically. The pressure gradient across the stenosis is estimated using the modified Bernoulli equation from the peak velocity obtained using continuous-wave Doppler (Fig. 11.42).[138] In patients with tricuspid regurgitation, the right ventricular systolic pressure can be calculated from the peak velocity of the tricuspid regurgitation jet. The pulmonary artery pressure can be estimated by subtracting the gradient across the stenosis from the right ventricular systolic pressure. After balloon pulmonary valvotomy, pulmonary regurgitation or restenosis can occur and can be diagnosed on TTE.

Left Ventricular Outflow Obstruction

As with right ventricular outflow obstruction, obstruction of flow from the left ventricle can occur at any level ranging from the outflow tract beneath the valve, to the valve itself, to the supravalvular region of the ascending aorta or in the descending thoracic aorta. The two least common types of outflow tract obstruction in adults are the subvalvular and the supravalvular forms. Subvalvular stenosis in adults is usually a result of a discrete subaortic membrane or ridge just beneath the valve. Discrete subaortic stenosis may be seen

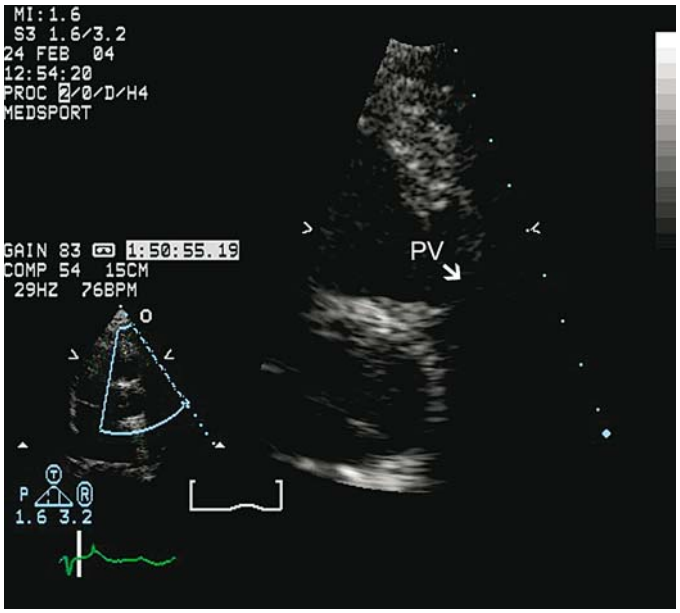

FIGURE 11.41. High parasternal view of the pulmonic valve (PV) in a patient with pulmonic stenosis. The leaflet tips have restricted motion causing characteristic doming in systole (arrow).

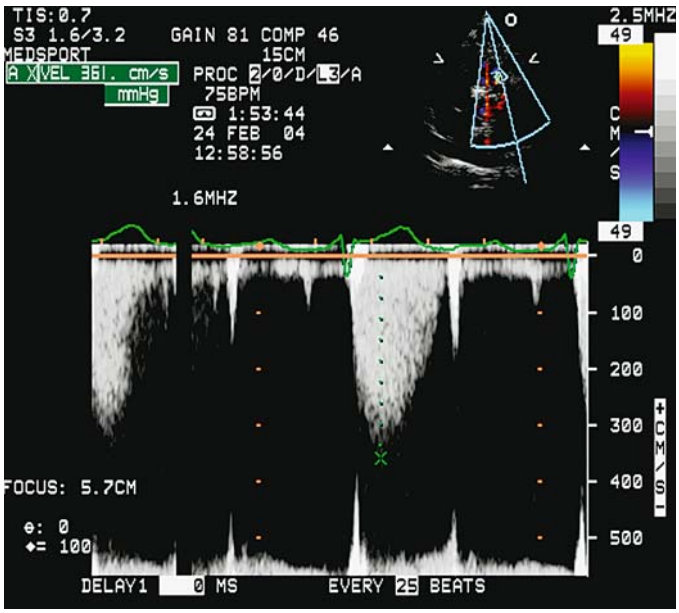

FIGURE 11.42. Continuous-wave Doppler across the pulmonic valve with a peak pressure gradient of 52 mmHg, consistent with moderate pulmonic stenosis.

in isolation or after surgical repair of congenital heart defects such as the AV canal. The membrane is identified on 2D TTE in the parasternal long axis or apical views as a linear echo originating from and perpendicular to the interventricular septum (Fig. 11.43). If the membrane itself is not seen, a high-velocity color jet in systole originating just below and directed toward the valve may raise suspicion of its existence. Continuous-wave Doppler permits estimation of severity of stenosis.[139–141] Some degree of aortic regurgitation caused by aortic leaflet trauma from the high-velocity stenotic jet is seen in up to 80% of patients in one study of 134 adults with the anomaly, but was more than mild in <20% of patients and did not appear to progress during a follow-up of 4.8 years.[142] This suggests that resection of mildly or moderately obstructive membranes is not necessary in asymptomatic patients as was previously recommended to prevent progression of aortic insufficiency. Two other forms of subvalvular stenosis, the fibromuscular type and the tunnel type, are infrequently seen in adults. Supravalvular stenosis may occur as a discrete membrane typically located at the sinotubular junction, as an hour-glass deformity of the ascending aorta (the most common type) associated with "elfin" facies and hypercalcemia as part of the Williams syndrome, or as diffuse hypoplasia of the ascending aorta and arch. Two-dimensional images from a high parasternal and suprasternal notch transducer locations may be necessary to view these defects.[143] Continuous-wave Doppler can accurately estimate the pressure gradient across discrete stenosis, but is unreliable if serial obstruction exists at multiple levels and in the tunnel form of supravalvular aortic stenosis.

Congenital aortic valve stenosis in adults is almost always a result of a bicuspid aortic valve that was normal at birth and became increasingly stenotic over time. Bicuspid aortic valves are the most common congenital cardiac anomaly occurring in 1% to 2% of the general population. Restricted motion of the leaflet tips relative to the body of the leaflet resulting in systolic doming of the valve in the parasternal long axis view may first suggest a bicuspid aortic valve. Valve morphology and leaflet number can be determined on 2D imaging from the parasternal short axis plane in most adults.[144,145] A true bicuspid aortic valve has two cusps (though a raphe may give the illusion of a third cusp) with two sinuses of Valsalva. Although a raphe may give the appearance of three cusps in diastole, valve opening in systole confirms the diagnosis when the two cusps are clearly seen. This is visualized especially well on TEE (Fig. 11.44). As with the other forms of left ventricular outflow obstruction, transvalvular pressure gradients derived from Doppler velocities can be used to estimate the severity of valvular aortic stenosis. Aortic valve area can be calculated using the continuity equation.[146] A rare abnormality of aortic valve anatomy is the quadricuspid aortic valve, which is more likely to be insufficient than stenotic (Fig. 11.45). The other two valve morphologies associated with congenital aortic stenosis, the

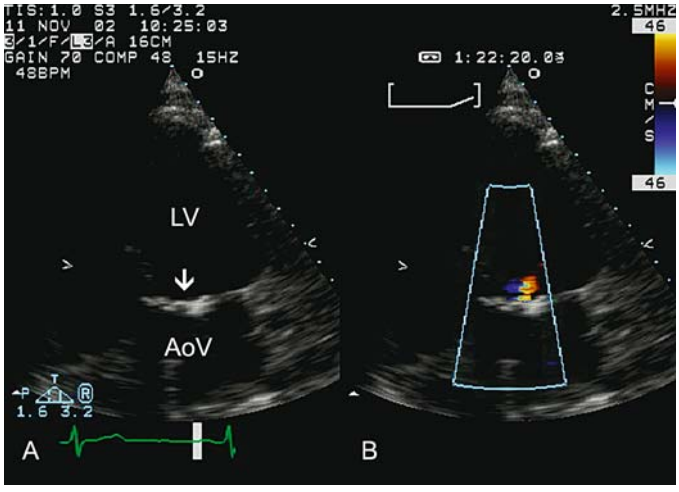

FIGURE 11.43. (A,B) Apical five-chamber view in a patient with discrete subaortic stenosis with aortic regurgitation. A bright linear echo of the ridge of tissue is seen below the aortic valve (arrow, A). A small jet of aortic insufficiency is noted in B.

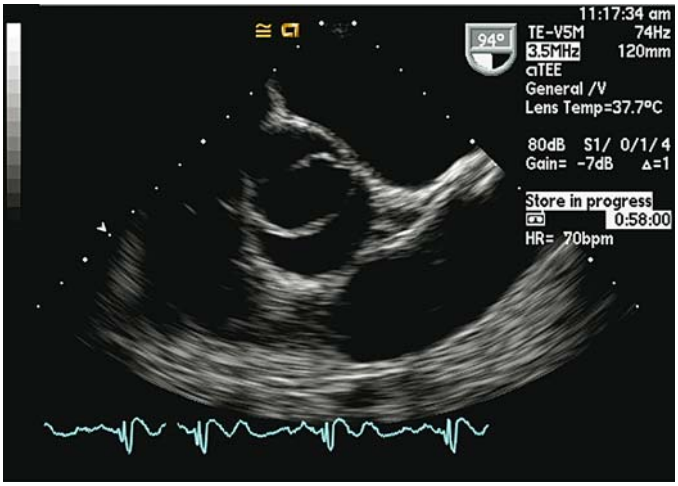

FIGURE 11.44. Transesophageal echocardiogram of a bicuspid aortic valve. There are two cusps and two sinuses of Valsalva in this valve.

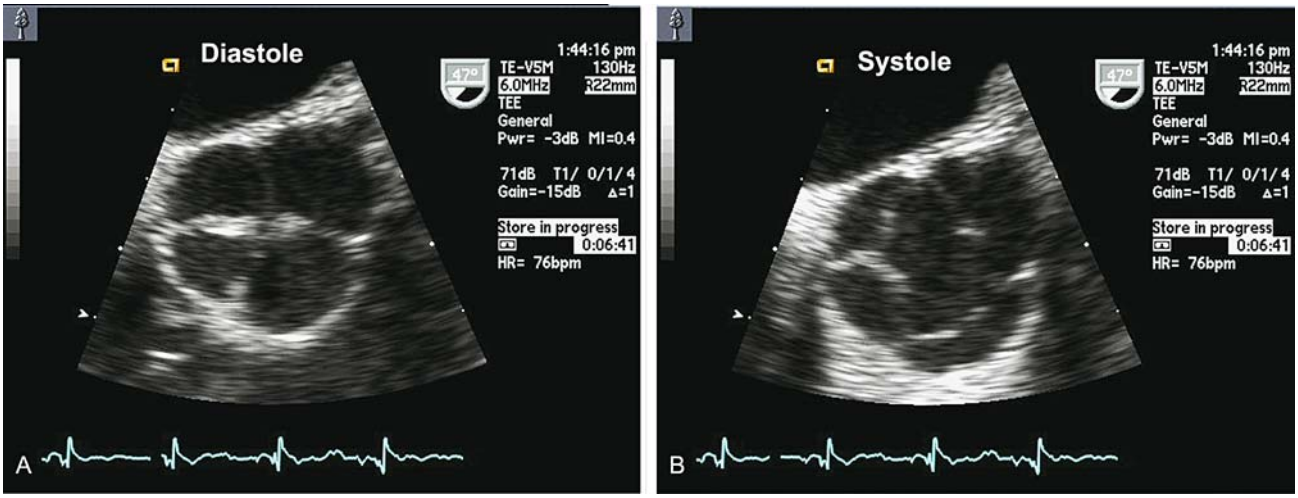

FIGURE 11.45. (A,B) A quadricuspid aortic valve is seen on a transesophageal echocardiogram short axis view in diastole (A) and systole (B).

acommissural valve and the unicuspid, unicommissural valve, are seen in children and rarely in the adult. Aortic stenosis in childhood is often treated by percutaneous balloon valvotomy, which may result in early or late aortic regurgitation and late restenosis that is readily diagnosed by 2D TTE. Some children with severe aortic stenosis or insufficiency undergo the Ross operation in which the diseased aortic valve is excised, the native pulmonary valve is transected and anastomosed to the aortic annulus, and a pulmonary homograft is placed in the pulmonary position. These patients should undergo serial echocardiographic surveillance for development of autograft dilation and insufficiency (Fig. 11.46).[147]

Coarctation of the aorta may take one of several forms, but is most commonly caused by a discrete shelf of tissue in the descending thoracic aorta just distal to the ostium of the left subclavian artery near the insertion of the ligamentum arteriosum. Approximately 80% to 85% of patients with coarctation of the aorta have a bicuspid aortic valve, though the opposite is not true. The coarct site is most likely to be visualized by 2D TTE from a suprasternal notch transducer position (Fig. 11.47) with a mosaic high velocity jet at the site of the stenosis on color Doppler.[148–150] However, the descending thoracic aorta distal to the coarctation may not be seen clearly in adults, thus obscuring the diagnosis. Color-guided continuous-wave Doppler provides an estimate of the gradient across the coarctation with certain caveats: (1) The gradient across the narrowing is flow dependent, so it may be lower when the patient is at rest. Exercise such as treadmill walking or leg lifts may increase the peak gradient across the coarct, but may also cause flow to continue across the stenosis into diastole, a sensitive indicator of more severe stenosis. (2) The coexistence of a patent ductus arteriosus with diversion of blood proximal to the coarct to the pulmonary artery causes the Doppler to underestimate the true gradient as will the presence of large or numerous collaterals around the coarctation. (3) Severe aortic stenosis from a bicuspid valve also results in falsely low gradient. A higher gradient may be revealed after aortic valve replacement. An example of continuous wave Doppler of severe coarctation is seen in Figure 11.48. Operative coarct repair in childhood may have been done by one of several methods, such as creation of a subclavian flap as a patch, excision of the coarct with reanastomosis of the proximal and distal aorta, or placement of an

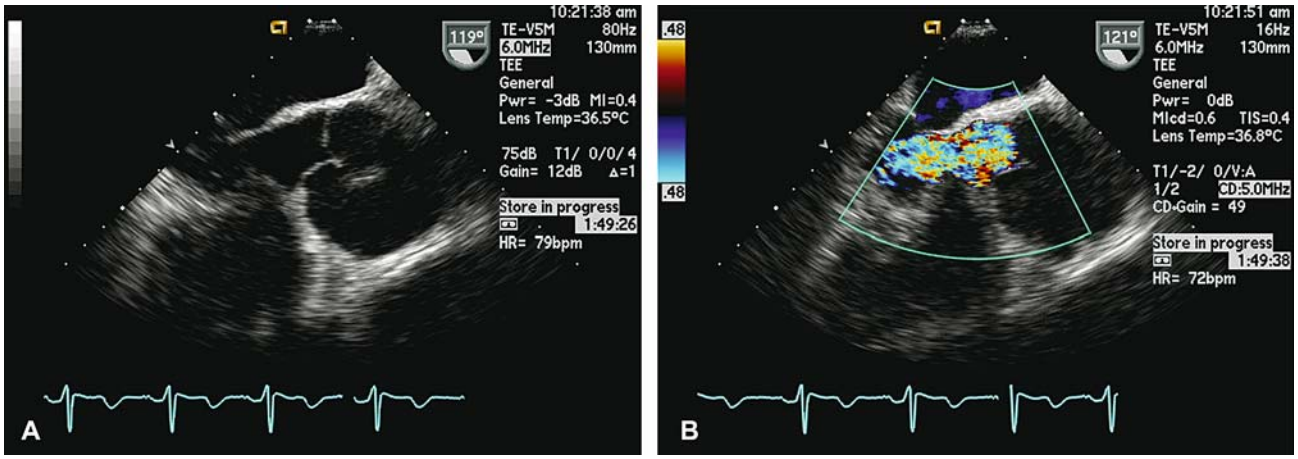

FIGURE 11.46. (A,B) Two-dimensional (A) and color Doppler (B) transesophageal echocardiogram of aortic valve and proximal aorta in a patient who has undergone the Ross operation. There is severe aortic insufficiency noted in the left ventricular outflow tract.

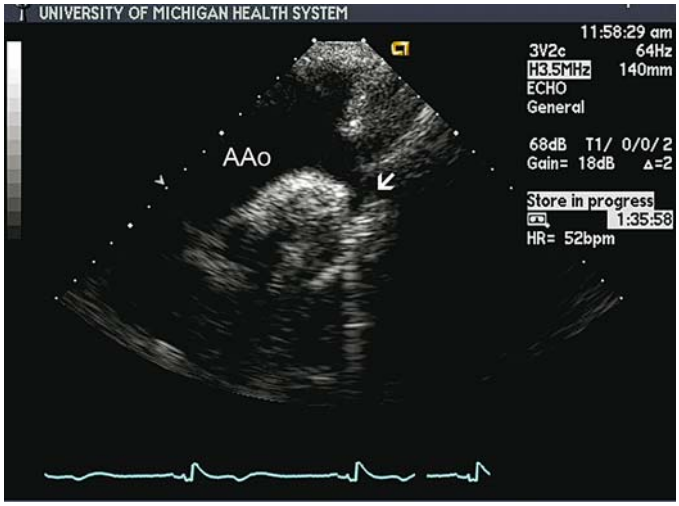

FIGURE 11.47. Suprasternal notch view in a patient with coarctation of the aorta. There is marked narrowing just distal to the takeoff of the left subclavian artery (arrow). The ascending aorta (AAo) is aneurysmal.

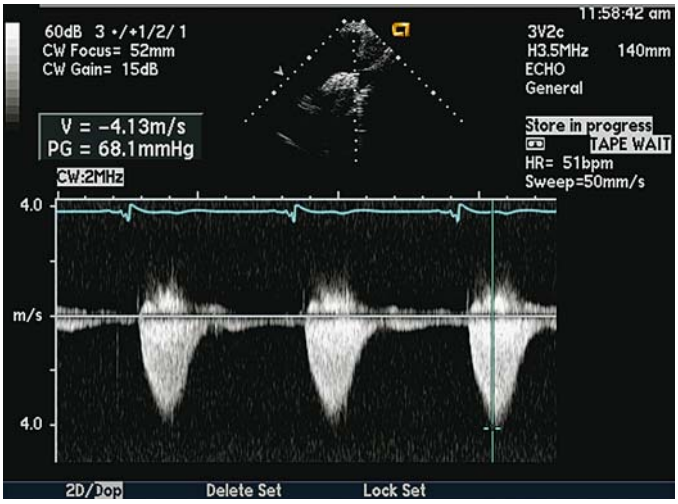

FIGURE 11.48. Continuous-wave Doppler through the coarctation site demonstrates a peak pressure gradient of 68 mm Hg.

interposition conduit. Knowledge of the type of repair is important to adequately assess for late problems. Potential late complications of coarct repair include restenosis of the coarct site and aneurysm of the descending aorta proximal to or just distal to the repair. In addition, aortic stenosis can develop as can aneurysms of the ascending aorta related to abnormalities of the media of the vessel wall. Transthoracic echocardiography and TEE can be used to visualize each of these complications or sequelae of coarctation of the aorta.

Miscellaneous Congenital Anomalies

Systemic to Pulmonary Artery Shunts

The most common native extracardiac left-to-right shunt seen in adults is the patent ductus arteriosus (PDA). The ductus arteriosus, which normally closes at birth, is a normal structure of the fetal vascular circuit that diverts blood from the pulmonary artery directly to the descending aorta bypassing the lungs. In certain individuals, particularly infants with other congenital cardiac defects or who are premature, the ductus may remain patent. The right-to-left shunt present *in utero* will reverse as pulmonary vascular resistance drops in the first week of life and a left-to-right shunt will ensue. The size of the shunt is determined by the diameter of the vascular connection and the pulmonary vascular resistance. In patients with large left-to-right shunts, the development of fixed pulmonary vascular disease will cause the shunt to again reverse with resultant differential cyanosis of the lower extremities. The ductal vessel is rarely seen directly in adults on TTE, but may be visualized in children from the suprasternal or high parasternal transducer location in the short axis view. It may be clearly seen on TEE (Fig. 11.49). In the typical patient with small PDA, a narrow high-velocity continuous color jet may be identified entering the main pulmonary artery adjacent to the left pulmonary artery directed retrograde to the pulmonary valve (Fig. 11.50). This is best

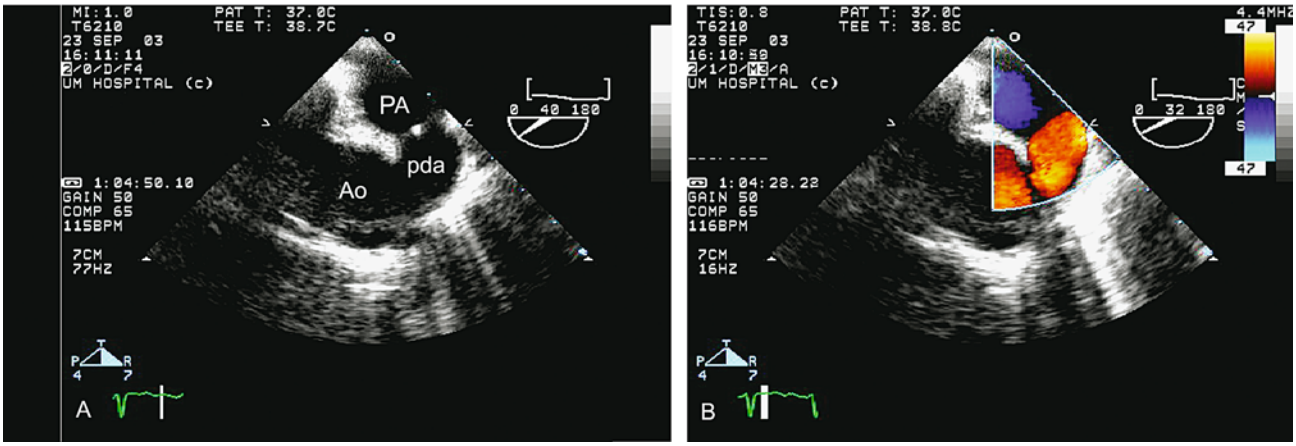

FIGURE 11.49. (A) A large patent ductus arteriosus (pda) is visualized connecting the descending thoracic aorta (Ao) and the pulmonary artery (PA). (B) A low-velocity jet is seen on color Doppler.

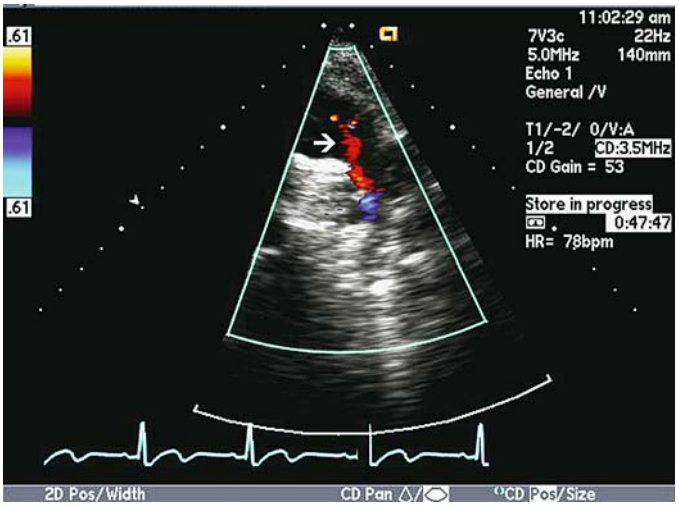

FIGURE 11.50. Color Doppler of the pulmonary artery in the high parasternal view shows a narrow jet (arrow) originating just proximal to the bifurcation of the pulmonary artery directed retrograde to the pulmonic valve.

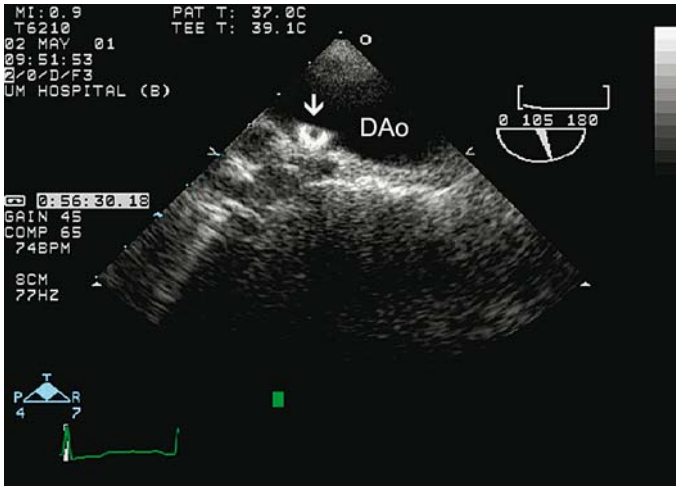

FIGURE 11.51. On transesophageal echocardiogram of the descending thoracic aorta (DAo) in the long axis plane, a bright circular structure is identified (arrow), which represents the distal aspect of a coil inserted into this patient's patent ductus arteriosus.

seen in the high parasternal imaging plane.[151–153] Continuous-wave Doppler of the descending aorta may reveal retrograde diastolic flow indicating left-to-right shunting through the ductus. Two-dimensional and Doppler TTE and TEE are also ideal for monitoring PDA during and after percutaneous closure (Fig. 11.51).[154]

Rarely, a sinus of Valsalva aneurysm, a result of localized weakening of the media of the sinus, may occur. On TTE, a sinus of Valsalva aneurysm is characterized by localized bulging of the sinus, often into the right ventricle (Fig. 11.52).[155] Color Doppler of unruptured aneurysms may demonstrate aortic regurgitation due to abnormal geometry of and failure of valve coaptation in diastole. The aneurysm may rupture into any cardiac chamber; aneurysms of the right coronary sinus typically rupture into the right ventricle and those of the noncoronary cusp rupture into the right atrium, resulting in a continuous left-to-right shunt easily imaged by color Doppler.[156–159] Transesophageal echocardiography may visualize the defect more clearly than TTE.[160]

The most common surgically constructed systemic-to-pulmonary shunts seen in the adult population are the Glenn anastomosis of the superior vena cava to the pulmonary artery, and the Blalock-Taussig shunt from either subclavian artery to the ipsilateral pulmonary artery. Generally, the conduit itself is not visualized on 2D imaging in adults; however, spectral Doppler can be used to assess the pressure across the circuit, and thus estimate pulmonary artery pressure.

Coronary Artery Abnormalities

Anomalous origin of coronary arteries occurs in approximately 1% of adults undergoing cardiac catheterization. The most common type is origin of the left circumflex from the right coronary sinus and is usually benign and discovered

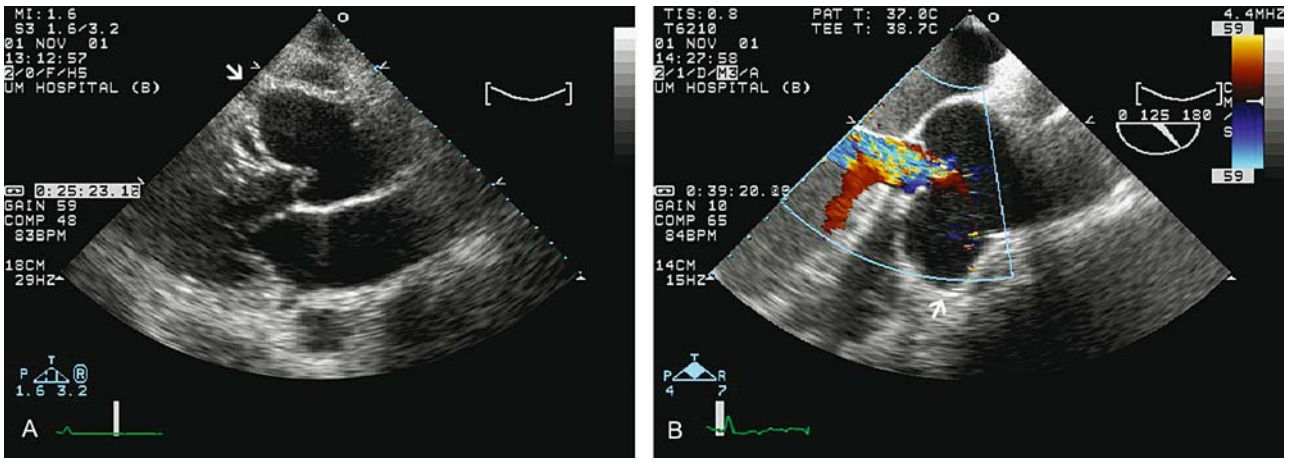

FIGURE 11.52. (A,B) Transesophageal echocardiogram in the long axis plane of a sinus of Valsalva aneurysm. The marked dilation of the sinus in each patient is noted (arrow, A and B). The aneurysm has distorted the aortic annulus in the patient in B, who has significant aortic insufficiency noted on color Doppler flow.

incidentally on coronary angiography. The variants associated with myocardial ischemia and death are the origin of the left main coronary artery from the right coronary artery passing between the two great arteries and origin of the left coronary artery from the pulmonary artery with reversal of coronary flow. Both of these entities may cause myocardial infarction and congestive heart failure. Transthoracic 2D imaging in the basal short axis plane at the level of the aorta may be useful for imaging coronary artery ostia in some adults.[161] In adults, TEE is far superior to TTE for localizing coronary ostia.[162–164] In some individuals, the proximal half of the artery may be seen. Coronary arterial fistulas may appear as turbulent jets on TEE or as hugely dilated vessels seen on TEE.[165–167]

Summary

Transthoracic echocardiography and transesophageal echocardiography are ideally suited for the initial diagnosis, management, and continued surveillance of adults with congenital heart defects. Indications for echocardiography in these patients have been established. The study should be performed in a deliberate, segmental fashion.

References

1. Warnes CA, Liberthson R, Danielson GK, et al. Task force 1: the changing profile of congenital heart disease in adult life. J Am Coll Cardiol 2001;37(5):1170–1175.
2. Hoffman JIE, Kaplan S, Liberthson RR. Prevalence of congenital heart disease. Am Heart J 2004;147:425–439.
3. Klewer SE, Samson RA, Donnerstein RL, Lax D, Zamora R, Goldberg SJ. Comparison of accuracy of diagnosis of congenital heart disease by history and physical examination versus echocardiography. Am J Cardiol 2002;89:1329–1331.
4. Marx GR. Doppler color flow echocardiography: indispensable application to congenital heart disease. Echocardiography 1995;12:413–424.
5. Miller-Hance WC, Silverman NH. Transesophageal echocardiography (TEE) in congenital heart disease with focus on the adult. Cardiol Clin 2000;18:861–892.
6. Masani ND. Transoesophageal echocardiography in adult congenital heart disease. Heart 2001;86(suppl 2):II30–II40.
7. Seward JB. Biplane and multiplane transesophageal echocardiography: evaluation of congenital heart disease. Am J Card Imaging 1995;9:129–136.
8. Peterson GE, Brickner ME, Reimold SC. Transesophageal echocardiography: clinical indications and applications. Circulation 2003;107:2398–2402.
9. Smallhorn JF. Intraoperative transesophageal echocardiography in congenital heart disease. Echocardiography 2002;19:709–723.
10. Bengur AR, Li JS, Herlong JR, Jaggers J, Sanders SP, Ungerleider RM. Intraoperative transesophageal echocardiography in congenital heart disease. Semin Thorac Cardiovasc Surg 1998;10:255–264.
11. Elzenga NJ. The role of echocardiography in transcatheter closure of atrial septal defects. Cardiol Young 2000;10:474–483.
12. Rigby ML. Transoesophageal echocardiography during interventional cardiac catheterization in congenital heart disease. Heart 2001;86(suppl 2):II23–II29.
13. Rhodes JF, Lane GK, Tuzcu EM, Latson LA. Invasive echocardiography: the use of catheter imaging by the interventional cardiologist. Catheter Cardiovasc Interv 2003;59:277–290.
14. Zanchetta M, Rigatelli G, Pedon L, Zennaro M, Maiolono P, Onorato E. Role of intracardiac echocardiography in atrial septal abnormalities. J Interv Cardiol 2003;16:63–77.
15. Rice MJ, McDonald RW, Li X, Shen I, Ungerleider RM, Sahn DJ. New technology and methodologies for intraoperative, perioperative, and intraprocedural monitoring of surgical and catheter interventions for congenital heart disease. Echocardiography 2002;19:725–734.
16. Mullen MJ, Dias BF, Walker F, Siu SC, Benson LN, McLaughlin PR. Intracardiac echocardiography guided device closure of atrial septal defects. J Am Coll Cardiol 2003;41:285–292.
17. Rhodes JF Jr, Qureshi AM, Preminger TJ, et al. Intracardiac echocardiography during transcatheter interventions for congenital heart disease. Am J Cardiol 2003;92:1482–1484.
18. Lange A, Palka P, Burstow DJ, Godman MJ. Three-dimensional echocardiography; historical development and current applications. J Am Soc Echocardiogr 2001;14:403–412.
19. Marx GR, Sherwood MC. Three-dimensional echocardiography in congenital heart disease; a continuum of unfulfilled promises? No. A presently clinically applicable technology with an important future? Yes. Pediatr Cardiol 2002;23:266–285.
20. Acar P. Three-dimensional echocardiography in transcatheter closure of atrial septal defects. Cardiol Young 2000;10:484–492.
21. Marx GR, Sherwood MC, Fleishman C, Van Praagh R. Three-dimensional echocardiography of the atrial septum. Echocardiography 2001;18:433–443.
22. Baweja G, Nanda NC, Kirklin JK. Definitive diagnosis of cor triatriatum with common atrium by three-dimensional echocardiography in an adult. Echocardiography 2004;21:303–306.
23. Kovalchin JP, Silverman NH. The impact of fetal echocardiography. Pediatr Cardiol 2004;25:299–306.
24. De Laat LE, Galema TW, Krenning BJ, Roelandt JR. Diagnosis of non-compaction cardiomyopathy with contrast echocardiography. Int J Cardiol 2004;94:127;129.
25. Cheitlin MS, Alpert JS, Armstrong WF, et al. ACC/AHA guidelines for the clinical application of echocardiography: a report of the American College of Cardiology/American Heart Association task force on practice guidelines (committee on clinical application of echocardiography) developed in collaboration with the American Society of Echocardiography. Circulation 1997;95:1686–1744.
26. Diamond MA, Dillon JC, Haine CL, et al. Echocardiographic features of atrial septal defect. Circulation 1971;43:129–135.
27. Meyer RA, Schwartz DC, Benzing G 3rd, Kaplan S. Ventricular septum in right ventricular volume overload: an echocardiographic study. Am J Cardiol 1972;30:349–353.
28. Radtke WE, Tajik AJ, Gau GT, Schattenberg TT, Giuliani ER, Tancredi RG. Atrial septal defect: echocardiographic observations. Studies in 120 patients. Ann Intern Med 1976;84:246–253.
29. Chazal RA, Armstrong WF, Dillon JC, Feigenbaum H. Diastolic ventricular septal motion in atrial septal defect: analysis of M-mode echocardiograms in 31 patients. Am J Cardiol 1983;52:1088–1090.
30. Weyman AE, Wann S, Feigenbaum H, Dillon JC. Mechanism of abnormal septal motion in patients with right ventricular volume overload: a cross-sectional echocardiographic study. Circulation 1976;54:179–186.
31. Shimada R, Takeshita A, Nakamura M. Noninvasive assessment of right ventricular systolic pressure in atrial septal defect: analysis of the end-systolic configuration of the

ventricular septum by two-dimensional echocardiography. Am J Cardiol 1984;53:1117–1123.
32. King ME, Braun H, Goldblatt A, Liberthson R, Weyman AE. Interventricular septal configuration as a predictor of right ventricular systolic hypertension in children: a cross-sectional echocardiographic study. Circulation 1983;68:68–75.
33. Ryan T, Petrovic O, Dillon JC, Feigenbaum H, Conley MJ, Armstrong WF. An echocardiographic index for separation of right ventricular volume and pressure overload. J Am Coll Cardiol 1985;5:918–927.
34. Kitabatake A, Inoue M, Asao M, et al. Noninvasive evaluation of the ratio of pulmonary to systemic flow in atrial septal defect by duplex Doppler echocardiography. Circulation 1984;69: 73–79.
35. Dittmann H, Jacksch R, Voelker W, Karsch KR, Seipel L. Accuracy of Doppler echocardiography in quantification of left to right shunts in adult patients with atrial septal defect. J Am Coll Cardiol 1988;11:338–342.
36. Mehta RH, Helmcke F, Nanda NC, Pinheiro L, Samdarshi TE, Shah VK. Uses and limitations of transthoracic echocardiography in the assessment of atrial septal defect in the adult. Am J Cardiol 1991;7:288–294.
37. Dillon JC, Weyman AE, Feigenbaum H, Eggleton RC, Johnston K. Cross-sectional echocardiographic examination of the interatrial septum. Circulation 1977;55:115–120.
38. Shub C, Dimopoulos IN, Seward JB, et al. Sensitivity of two-dimensional echocardiography in the direct visualization of atrial septal defect utilizing the subcostal approach: experience with 154 patients. J Am Coll Cardiol 1983;2:127–135.
39. Valdes-Cruz LM, Pieroni DR, Roland JM, Varghese PJ. Echocardiographic detection of intracardiac right-to-left shunts following peripheral vein injections. Circulation 1976;54: 558–562.
40. Serruys PW, van den Brand M, Hugenholtz PG, Roelandt J. Intracardiac right-to-left shunts demonstrated by two-dimensional echocardiography after peripheral vein injection. Br Heart J 1979;42:429–437.
41. Fraker TD Jr, Harris PJ, Behar VS, Kisslo JA. Detection and exclusion of interatrial shunts by two-dimensional echocardiography and peripheral venous injection. Circulation 1979; 59:379–384.
42. Lynch JJ, Schuchard GH, Gross CM, Wann LS. Prevalence of right-to-left atrial shunting in a healthy population: detection by Valsalva maneuver contrast echocardiography. Am J Cardiol 1984;53:1478–1480.
43. Weyman AE, Wann LS, Caldwell RL, Hurwitz RA, Dillon JC, Feigenbaum H. Negative contrast echocardiography: a new method for detecting left-to-right shunts. Circulation 1979;59: 498–505.
44. Siostrzonek P, Lang W, Zangeneh M, et al. Significance of left-sided heart disease for the detection of patent foramen ovale by transesophageal contrast echocardiography. J Am Coll Cardiol 1992;19:1192–1196.
45. Hausmann D, Mugge A, Becht I, Daniel WG. Diagnosis of patent foramen ovale by transesophageal echocardiography and association with cerebral and peripheral embolic events. Am J Cardiol 1992;70:668–672.
46. de Belder MA, Tourikis L, Griffith M, Leech G, Camm AJ. Transesophageal contrast echocardiography and color flow mapping: methods of choice for the detection of shunts at the atrial level? Am Heart J 1992;124:1545–1550.
47. Stollberger C, Schneider B, Abzieher F, Wollner T, Meinertz T, Slany J. Diagnosis of patent foramen ovale by transesophageal contrast echocardiography. Am J Cardiol 1993;71:604–606.
48. Lechat P, Mas JL, Lascault G, et al. Prevalence of patent foramen ovale in patients with stroke. N Engl J Med 1988;318: 1148–1152.
49. Pearson AC, Labovitz AJ, Tatineni S, Gomez CR. Superiority of transesophageal echocardiography in detecting cardiac source of embolism in patients with cerebral ischemia of uncertain etiology. J Am Coll Cardiol 1991;17:66–72.
50. Pearson AC, Nagelhout D, Castello R, Gomez CR, Labovitz AJ. Atrial septal aneurysm and stroke: a transesophageal echocardiographic study. J Am Coll Cardiol 1991;18:1223–1229.
51. Siostrzonek P, Zangeneh M Gossinger H, et al. Comparison of transesophageal and transthoracic contrast echocardiography for detection of a patent foramen ovale. Am J Cardiol 1991; 68:1247–1249.
52. Mas JL, Arquizan C, Lamy C, et al. Patent foramen ovale and atrial septal aneurysm study group. Recurrent cerebrovascular events associated with patent foramen ovale, atrial septal aneurysm, or both. N Engl J Med 2001;345:1740–1746.
53. Mehta RH, Helmcke F, Nanda NC, Hsiung M, Pacifico AD, Hsu TL. Transesophageal Doppler color flow mapping assessment of atrial septal defect. J Am Coll Cardiol 1990;16:1010–1016.
54. Hanrath P, Schluter M, Langenstein B, et al. Detection of ostium secundum atrial septal defects by transoesophageal cross-sectional echocardiography. Br Heart J 1983;49:350–358.
55. Kronzon I, Tunick PA, Freedberg RS, Trehan N, Rosenzweig BP, Schwinger ME. Transesophageal echocardiography is superior to transthoracic echocardiography in the diagnosis of sinus venosus atrial septal defect. J Am Coll Cardiol 1991;17: 537–542.
56. Pascoe RD, Oh JK, Warnes CA, et al. Heart disease in the young: diagnosis of sinus venosus atrial septal defect with transesophageal echocardiography. Circulation 1996;94: 1049–1055.
57. Shub C, Tajik AJ, Seward JB, Hagler DJ, Danielson GK. Surgical repair of uncomplicated atrial septal defect without "routine" preoperative cardiac catheterization. J Am Coll Cardiol 1985; 6:49–54.
58. Lipshultz SE, Sanders SP, Mayer JE, Colan SD, Lock JE. Are routine preoperative cardiac catheterization and angiography necessary before repair of ostium primum atrial septal defect? J Am Coll Cardiol 1988;11:373–378.
59. Prokselj K, Kozelj M, Zadnik V, Podnar T. Echocardiographic characteristics of secundum-type atrial septal defects in adult patients: implications for percutaneous closure using Amplatzer septal occluders. J Am Soc Echocardiogr 2004; 17:1167–1172.
60. Carcagni A, Presbitero P. New echocardiographic diameter for Amplatzer sizing in adult patients with secundum atrial septal defect: preliminary results. Catheter Cardiovasc Intervent 2004;62:409–414.
61. Tamborini G, Pepi M, Susini F, et al. Comparison of two- and three-dimensional transesophageal echocardiography in patients undergoing atrial septal closure with the Amplatzer septal occluder. Am J Cardiol 2002;90:1025–1028.
62. Koenig P, Cao QL, Heitschmidt M, Waight DJ, Hijazi ZM. Role of intracardiac echocardiographic guidance in transcatheter closure of atrial septal defects and patent foramen ovale using the Amplatzer device. J Intervent Cardiol 2003;16: 51–62.
63. Zanchetta M, Rigatelli G, Onorato E. Intracardiac echocardiography and transcranial Doppler ultrasound to guide closure of patent foramen ovale. J Invasive Cardiol 2003;15:93–96.
64. Alboliras ET, Hijazi ZM. Comparison of costs of intracardiac echocardiography and transesophageal echocardiography in monitoring percutaneous device closure of atrial septal defect in children and adults. Am J Cardiol 2004;94: 690–692.
65. Bierman FZ, Fellows K, Williams RG. Prospective identification of ventricular septal defects in infancy using subxiphoid

two-dimensional echocardiography. Circulation 1980;62:807–817.
66. Sutherland GR, Godman MJ, Smallhorn JF, et al. Ventricular septal defects. Two dimensional echocardiographic and morphological correlations. Br Heart J 1982;47:316–328.
67. Capelli H, Andrade J, Somerville J. Classification of the site of ventricular septal defect by 2-dimensional echocardiography. Am J Cardiol 1983;51:1474–1480.
68. Pieroni DR, Nishimura RA, Bierman FZ, et al. Second natural history study of congenital heart defects. Ventricular septal defect: echocardiography. Circulation 1993;87(2 suppl):I80–88.
69. Canale JM, Sahn DJ, Allen HD, Goldberg SJ, Valdes-Cruz LM, Ovitt TW. Factors affecting real-time, cross-sectional echocardiographic imaging of perimembranous ventricular septal defects. Circulation 1981;63:689–697.
70. Ludomirsky A, Huhta JC, Vick GW 3rd, Murphy DJ Jr, Danford DA, Morrow WR. Color Doppler detection of multiple ventricular septal defects. Circulation 1986;74:1317–1322.
71. Grenadier E, Shem-Tov A, Motro M, Palant A. Echocardiographic diagnosis of left ventricular-right atrial communication. Am Heart J 1983;106:407–409.
72. Canale JM, Sahn DJ, Valdes-Cruz L, Allen HD, Goldberg SJ, Ovitt TW. Accuracy of two-dimensional echocardiography in the detection of aneurysms of the ventricular septum. Am Heart J 1982;101:255–259.
73. Murphy DJ Jr, Ludomirsky A, Huhta JC. Continuous-wave Doppler in children with ventricular septal defect: noninvasive estimation of interventricular pressure gradient. Am J Cardiol 1986;57:428–432.
74. Ge Z, Zhang Y, Kang W, Fan D, An F. Noninvasive evaluation of interventricular pressure gradient across ventricular septal defect: a simultaneous study of Doppler echocardiography and cardiac catheterization. Am Heart J 1992;124:176–182.
75. Ge Z, Zhang Y, Kang W, Fan D, Ji X, Duran C. Noninvasive evaluation of right ventricular and pulmonary artery systolic pressures in patients with ventricular septal defects: simultaneous study of Doppler and catheterization data. Am Heart J 1993;125:1073–1081.
76. Andrade JL, Serino W, de Leval M, Somerville J. Two-dimensional echocardiographic assessment of surgically closed ventricular septal defect. Am J Cardiol 1983;52:325–329.
77. Mostow N, Riggs T, Borkat G. Echocardiographic features of ventricular septal defect patch dehiscence. Am Heart J 1981;102:941–942.
78. Aziz KU, Cole RB, Paul MH. Echocardiographic features of supracristal ventricular septal defect with prolapsed aortic valve leaflet. Am J Cardiol 1979;43:854–859.
79. Agathangelou NE, dos Santos LA, Lewis BS. Real-time 2-dimensional echocardiographic imaging of right-sided cardiac vegetations in ventricular septal defect. Am J Cardiol 1983; 52:420–421.
80. Pedra CA, Pedra SR, Esteves CA, Chamie F, Christiani LA, Fontes VF. Transcatheter closure of perimembranous ventricular septal defects. Exp Rev Cardiovasc Ther 2004;2:253–264.
81. Arora R, Trehan V, Thakur AK, Mehta V, Sengupta PP, Nigam M. Transcatheter closure of congenital muscular ventricular septal defect. J Intervent Cardiol 2004;17:109–115.
82. Anderson RH, Ho SY, Falcao S, Daliento L, Rigby ML. The diagnostic features of atrioventricular septal defect with common atrioventricular junction. Cardiol Young 1998;8: 33–49.
83. Gonzalez-Juanatey C, Testa A, Vidan J, et al. Persistent left superior vena cava draining into the coronary sinus: report of 10 cases and literature review. Clin Cardiol 2004;27:515–518.
84. Snider AR, Ports TA, Silverman NH. Venous anomalies of the coronary sinus: detection by M-mode, two-dimensional and contrast echocardiography. Circulation 1979;60:721–727.
85. Stewart JA, Fraker TD Jr, Slosky DA, Wise NK, Kisslo JA. Detection of persistent left superior vena cava by two-dimensional contrast echocardiography. J Clin Ultrasound 1979;7:357–360.
86. Hibi N, Fukui Y, Nishimura K, Miwa A, Kambe T, Sakamoto N. Cross-sectional echocardiographic study on persistent left superior vena cava. Am Heart J 1980;100:69–76.
87. Foale R, Bourdillon PD, Somerville J, Rickards A. Anomalous systemic venous return: recognition by two-dimensional echocardiography. Eur Heart J 1983;4:186–915.
88. Wong ML, McCrindle BW, Mota C, Smallhorn JF. Echocardiographic evaluation of partial anomalous pulmonary venous drainage. J Am Coll Cardiol 1995;26:503–507.
89. Obeid AI, Carlson RJ. Evaluation of pulmonary vein stenosis by transesophageal echocardiography. J Am Soc Echocardiogr 1995;8:888–896.
90. Ammash NM, Seward JB, Warnes CA, Connolly HM, O'Leary PW, Danielson GK. Partial anomalous pulmonary venous connection: diagnosis by transesophageal echocardiography. J Am Coll Cardiol 1997;29:1351–1358.
91. Idris MT. Diagnostic aid of transesophageal echocardiography in an adult case of scimitar syndrome: confirmation of the findings at surgery and review of the literature. J Am Soc Echocardiogr 1998;11:387–392.
92. Oliver JM, Gallego P, Gonzalez A, Dominguez FJ, Aroca A, Mesa JM. Sinus venosus syndrome: atrial septal defect or anomalous venous connection? A multiplane transoesophageal approach. Heart 2002;88:634–638.
93. Kinnaird TD, Uzun O, Munt BI, Thompson CR, Yeung-Lai-Wah JA. Transesophageal echocardiography to guide pulmonary vein mapping and ablation for atrial fibrillation. J Am Soc Echocardiogr 2004;17:769–774.
94. Obeid AI, Carlson RJ. Evaluation of pulmonary vein stenosis by transesophageal echocardiography. J Am Soc Echocardiogr 1995;8:888–896.
95. Attie F, Rosas M, Rijlaarsdam M, et al. The adult patient with Ebstein anomaly: outcome in 72 unoperated patients. Medicine 2000;79:27–36.
96. Matsumoto M, Matsuo H, Nagata S, Hamanaka Y, Fujita T. Visualization of Ebstein's anomaly of the tricuspid valve by two-dimensional and standard echocardiography. Circulation 1976;53:59–79.
97. Shiina A, Seward JB, Edwards WD, Hagler DJ, Tajik AJ. Two-dimensional echocardiographic spectrum of Ebstein's anomaly: detailed anatomic assessment. J Am Coll Cardiol 1984;3(2 pt 1):356–370.
98. Gussenhoven EJ, Stewart PA, Becker AE, Essed CE, Ligtvoet KM, De Villeneuve VH. "Offsetting" of the septal tricuspid leaflet in normal hearts and in hearts with Ebstein's anomaly. Anatomic and echographic correlation. Am J Cardiol 1984; 54:172–176.
99. Quaegebeur JM, Sreeram N, Fraser AG, et al. Surgery for Ebstein's anomaly: the clinical and echocardiographic evaluation of a new technique. J Am Coll Cardiol 1991;17:722–728.
100. Canedo MI, Stefadouros MA, Frank MJ, Moore HV, Cundey DW. Echocardiographic features of cor triatriatum. Am J Cardiol 1977;40:615–619.
101. Ostman-Smith I, Silverman NH, Oldershaw P, Lincoln C, Shinebourne EA. Cor triatriatum sinistrum. Diagnostic features on cross-sectional echocardiography. Br Heart J 1984; 51:211–219.
102. Weindorf S, Goldberg H, Goldman M, Reitman M. Diagnosis of cor triatriatum by two-dimensional echocardiography. J Clin Ultrasound 1981;9:97–100.
103. Vuocolo LM, Stoddard MF, Longaker RA. Transesophageal two-dimensional and Doppler echocardiographic diagnosis of cor triatriatum in the adult. Am Heart J 1992;124:791–793.

104. Horowitz MD, Zager W, Bilsker M, Perryman RA, Lowery MH. Cor triatriatum in adults. Am Heart J 1993;126:472–474.
105. van Son JA, Danielson GK, Schaff HV, et al. Cor triatriatum: diagnosis, operative approach, and late results. Mayo Clin Proc 1993;68:854–859.
106. Rorie M, Xie GY, Miles H, Smith MD. Diagnosis and surgical correction of cor triatriatum in an adult: combined use of transesophageal echocardiography and catheterization. Catheter Cardiovasc Intervent 2000;51:83–86.
107. Driscoll DJ, Gutgesell HP, McNamara DG. Echocardiographic features of congenital mitral stenosis. Am J Cardiol 1978; 42:259–266.
108. Smallhorn J, Tommasini G, Deanfield J, Douglas J, Gibson D, Macartney F. Congenital mitral stenosis. Anatomical and functional assessment by echocardiography. Br Heart J 1981;45: 527–534.
109. Grenadier E, Sahn DJ, Valdes-Cruz LM, Allen HD, Oliveira Lima C, Goldberg SJ. Two-dimensional echo Doppler study of congenital disorders of the mitral valve. Am Heart J 1984; 107:319–325.
110. Williams RG. Echocardiography in the management of single ventricle: fetal through adult life. Echocardiography 1993;10: 331–342.
111. Coon PD, Rychik J, Novello RT, Ro PS, Gaynor W, Spray TL. Thrombus formation after the Fontan operation. Ann Thorac Surg 2001;71:1990–1994.
112. Balling G, Vogt M, Kaemmerer H, Eicken A, Meisner H, Hess J. Intracardiac thrombus formation after the Fontan operation. J Thorac Cardiovasc Surg 2000;119:745–752
113. Varma C, Warr MR, Hendler AL, Paul NS, Webb GD, Thierren J. Prevalence of "silent" pulmonary emboli in adults after the Fontan operation. J Am Coll Cardiol 2003;41:2252–2258.
114. Lopez-Fernandez T, Garcia-Fernandez MA, Perez David E, Moreno Yanguela M. Usefulness of contrast echocardiography in arrhythmogenic right ventricular dysplasia. J Am Soc Echocardiogr 2004;17:391–393.
115. Lindstrom L, Wilkenshoff UM, Larsson H, Wranne B. Echocardiographic assessment of arrhythmogenic right ventricular cardiomyopathy. Heart 2001;86:31–38.
116. Jenni R, Oeschlin E, Schneider J, Jost CA, Kaufmann PA. Echocardiographic and pathoanatomical characteristics of isolated left ventricular non-compaction: a step towards classification as a distinct cardiomyopathy. Heart 2001;86: 666–671.
117. Caldwell RL, Weyman AE, Hurwitz RA, Girod DA, Feigenbaum H. Right ventricular outflow tract assessment by cross-sectional echocardiography in tetralogy of Fallot. Circulation 1979;59:395–402.
118. Henry WL, Maron BJ, Griffith JM. Cross-sectional echocardiography in the diagnosis of congenital heart disease. Identification of the relation of the ventricles and great arteries. Circulation 1977;56:267–273.
119. Sanders SP, Bierman FZ, Williams RG. Conotruncal malformations: diagnosis in infancy using subxiphoid 2-dimensional echocardiography. Am J Cardiol 1982;50:1361–1367.
120. Di Segni E, Einzig S, Bass JL, Edwards JE. Congenital absence of pulmonary valve associated with tetralogy of Fallot: diagnosis by 2-dimensional echocardiography. Am J Cardiol 1983;51:1798–1800.
121. Jureidini SB, Appleton RS, Nouri S. Detection of coronary artery abnormalities in tetralogy of Fallot by two-dimensional echocardiography. J Am Coll Cardiol 1989;14:960–967.
122. Li W, Davlouros PA, Kilner PJ et al. Doppler-echocardiographic assessment of pulmonary regurgitation in adults with repaired tetralogy of Fallot: comparison with cardiovascular magnetic resonance imaging. Am Heart J 2004;147:165–172.
123. Therrien J, Siu SC, McLaughlin PR, Liu PP, Williams WG, Webb GD. Pulmonary valve replacement in adults late after repair of tetralogy of Fallot: are we operating too late? J Am Coll Cardiol 2000;36(5):1670–1675.
124. Mahle WT, Parks WJ, Fyfe DA, Sallee D. Tricuspid regurgitation in patients with repaired tetralogy of Fallot and its relation to right ventricular dilatation. Am J Cardiol 2003;92: 643–645.
125. Niwa K, Siu SC, Webb GD, Gatzoulis MA. Progressive aortic root dilation in adults later after repair of tetralogy of Fallot. Circulation 2002;106:1374–1378.
126. Gatzoulis MA, Clark AL, Cullen S, Newman CG, Redington AN. Right ventricular diastolic dysfunction 15 to 35 years after repair of tetralogy of Fallot. Restrictive physiology predicts superior exercise performance. Circulation 1995;91:1775–1781.
127. Aziz KU, Paul MH, Bharati S, Cole RB, Muster AJ, Lev M, Idriss FS. Two dimensional echocardiographic evaluation of Mustard operation for d-transposition of the great arteries. Am J Cardiol 1981;47:654–664.
128. Stumper O, Witsenburg M, Sutherland GR, Cromme-Dijkhuis A, Godman MJ, Hess J. Transesophageal echocardiographic monitoring of interventional cardiac catheterization in children. J Am Coll Cardiol 1991;18:1506–1514.
129. Maclellan-Tobert SG, Cetta F, Hagler DJ. Use of intravascular stents for superior vena cava obstruction after Mustard operation. Mayo Clin Proc 1996;71:1071–1076.
130. Wilson NJ, Neutze JM, Rutland MD, Ramage MC. Transthoracic echocardiography for right ventricular function late after the Mustard operation. Am Heart J 1996;131:360–367.
131. Duncan WJ, Freedom RM, Rowe RD, Olley PM, Williams WG, Trusler GA. Echocardiographic features before and after the Jatene procedure (anatomical correction) for transposition of the great vessels. Am Heart J 1981;102:227–232.
132. Beauchesne LM, Warnes CA, Connolly HM, Ammash NM, Tajik AJ, Danielson GK. Outcome of the unoperated adult who presents with congenitally corrected transposition of the great arteries. J Am Coll Cardiol 2002;40:285–290.
133. Mills P, Wolfe C, Redwood D, Leech G, Craige E, Leatham A. Non-invasive diagnosis of subpulmonary outflow tract obstruction. Br Heart J 1980;43:276–283.
134. Von Doenhoff LJ, Nanda NC. Obstruction within the right ventricular body: two-dimensional echocardiographic features. Am J Cardiol 1983;51:1498–1501.
135. Weyman AE, Hurwitz R,. Girod DA, Dillon JC, Feigenbaum H. Green D. Cross-sectional echocardiographic visualization of the stenotic pulmonary valve. Circulation 1977;56:769–774.
136. Weyman AE, Dillon JC, Feigenbaum H, Chang S. Echocardiographic patterns of pulmonary valve motion in valvular pulmonary stenosis. Am J Cardiol 1974;34(6):644–651.
137. Tinker DD, Nanda NC, Harris JP, Manning JA. Two-dimensional echocardiographic identification of pulmonary artery branch stenosis. Am J Cardiol 1982;50:814–820.
138. Lima CO, Sahn DJ, Valdes-Cruz LM, et al. Noninvasive prediction of transvalvular pressure gradient in patients with pulmonary stenosis by quantitative two-dimensional echocardiographic Doppler studies. Circulation 1983;67:866–871.
139. Hatle L. Noninvasive assessment and differentiation of left ventricular outflow obstruction with Doppler ultrasound. Circulation 1981;64:381–387.
140. Lima CO, Sahn DJ, Valdes-Cruz LM, et al. Prediction of the severity of left ventricular outflow tract obstruction by quantitative two-dimensional echocardiographic Doppler studies. Circulation 1983;68:348–354.
141. Krueger SK, French JW, Forker AD, Caudill CC, Popp RL. Echocardiography in discrete subaortic stenosis. Circulation 1979;59:506–513.

142. Oliver JM, Gonzalez A, Gallego P, Sanchez-Recalde A, Benito F, Mesa JM. Discrete subaortic stenosis in adults: increased prevalence and slow rate of progression of the obstruction and aortic regurgitation. J Am Coll Cardiol 2001;38:835–842.
143. Weyman AE, Caldwell RL, Hurwitz RA, et al. Cross-sectional echocardiographic characterization of aortic obstruction. 1. Supravalvular aortic stenosis and aortic hypoplasia. Circulation 1978;57:491–497.
144. Brandenburg RO Jr, Tajik AJ, Edwards WD, Reeder GS, Shub C, Seward JB. Accuracy of 2–dimensional echocardiographic diagnosis of congenitally bicuspid aortic valve: echocardiographic-anatomic correlation in 115 patients. Am J Cardiol 1983;51: 1469–1473.
145. Zema MJ, Caccavano M. Two dimensional echocardiographic assessment of aortic valve morphology: feasibility of bicuspid valve detection. Prospective study of 100 adult patients. Br Heart J 1982;48:428–433.
146. Kosturakis D, Allen HD, Goldberg SJ, Sahn DJ, Valdes-Cruz LM. Noninvasive quantification of stenotic semilunar valve areas by Doppler echocardiography. J Am Coll Cardiol 1984;3: 1256–1262.
147. Xie GY, Bhakta D, Smith MD. Echocardiographic follow-up study of the Ross procedure in older versus younger patients. Am Heart J 2001;142:331–335.
148. Weyman AE, Caldwell RL, Hurwitz RA, et al. Cross-sectional echocardiographic detection of aortic obstruction. 2. Coarctation of the aorta. Circulation 1978;57:498–502.
149. Smallhorn JF, Huhta JC, Adams PA. Cross-sectional echocardiographic assessment of coarctation in the sick neonate and infant. Br Heart J 1983;50:349–361.
150. Huhta JC, Gutgesell HP, Latson LA, Huffines FD. Two-dimensional echocardiographic assessment of the aorta in infants and children with congenital heart disease. Circulation 1984;70:417–424.
151. Perez JE, Nordlicht SC, Geltman EM. Patent ductus arteriosus in adults: diagnosis by suprasternal and parasternal pulsed Doppler echocardiography. Am J Cardiol 1984;53:1473–1475.
152. Cloez JL, Isaaz K, Pernot C. Pulsed Doppler characteristics of ductus arteriosus in infants associated with congenital anomalies of the heart or great arteries. Am J Cardiol 1986;56:845–851.
153. Swensson RE, Valdes-Cruz LM, Sahn D, et al. Real-time Doppler color flow mapping for detection of patent ductus arteriosus. J Am Coll Cardiol 1986;8:1105–1112.
154. Bridges ND, Perry SB, Parness I, Keane JF, Lock JE. Transcatheter closure of a large patent ductus arteriosus with the clamshell septal umbrella. J Am Coll Cardiol 1991;18:1297–1302.
155. Terdjman M, Bourdarias JP, Farcot JC, et al. Aneurysms of sinus of Valsalva: two-dimensional echocardiographic diagnosis and recognition of rupture into the right heart cavities. J Am Coll Cardiol 1984;3:1227–1235.
156. Kiefaber RW, Tabakin BS, Coffin LH, Gibson TC. Unruptured sinus of Valsalva aneurysm with right ventricular outflow tract obstruction diagnosed by two-dimensional and Doppler echocardiography. J Am Coll Cardiol 1986;7:438–442.
157. Chow LC, Dittrich HC, Dembitsky WP, Nicod PH. Accurate localization of ruptured sinus of Valsalva aneurysm by real-time two-dimensional Doppler-flow imaging. Chest 1988;94: 462–465.
158. Chia BI, Ee BK, Choo MH, Yan PC. Ruptured aneurysm of sinus of Valsalva: recognition of Doppler color-flow mapping. Am Heart J 1988;115:686–688.
159. Goudevenos J, Kouvaras G, Chronopoulos DG, et al. Color Doppler echocardiography in the diagnosis of ruptured aneurysm of sinus of Valsalva. Eur Heart J 1990;11:666–669.
160. Rubin DC, Carliner NH, Salter DR, Plotnick GD, Hawke MW. Unruptured sinus of Valsalva aneurysm diagnosed by transesophageal echocardiography. Am Heart J 1992;124:225–227.
161. Kessler KM, Feldman T, Harding L, et al. Anomalous origin of the right coronary artery from the left sinus of Valsalva: echocardiographic-angiographic correlations. Am Heart J 1988;115:470–473.
162. Gaither NS, Rogan KM, Stajduhar K, et al. Anomalous origin and course of coronary arteries in adults: identification and improved imaging utilizing transesophageal echocardiography. Am Heart J 1991;122:69–75.
163. Smolin MR, Gorman PD, Gaither NS, Wortham DC. Origin of the right coronary artery from the left main coronary artery identified by transesophageal echocardiography. Am Heart J 1992;123:1062–1065.
164. Samdarshi TE, Hill DL, Nanda NC. Transesophageal color Doppler diagnosis of anomalous origin of the left circumflex coronary artery. Am Heart J 1991;122:571–573.
165. Velvis H, Schmidt KG, Silverman NH, Turley K. Diagnosis of coronary artery fistula by two-dimensional, pulsed Doppler ultrasound and color flow mapping. J Am Coll Cardiol 1989; 14:968–972.
166. Nishiguchi T, Matsuoka Y, Sennari E, et al. Congenital coronary artery fistula: diagnosis by two-dimensional Doppler echocardiography. Am Heart J 1990;120:1244–1248.
167. Samdarshi TE, Mahan EF III, Nanda NC, Sanyal RS. Transesophageal echocardiographic assessment of congenital coronary artery to coronary sinus fistulas in adults. Am J Cardiol 1991;68:263–266.